

Testing the Muon $g-2$ Anomaly at the LHC

A. Freitas¹, J. Lykken², S. Kell¹, and S. Westhoff¹

¹ PITTsburgh Particle-physics Astro-physics & Cosmology Center (PITT-PACC),
Department of Physics & Astronomy, University of Pittsburgh, Pittsburgh, PA 15260, USA

² Theoretical Physics Department, Fermilab, P.O. Box 500, Batavia, IL 60510, USA

Abstract

The long-standing difference between the experimental measurement and the standard-model prediction for the muon's anomalous magnetic moment, $a_\mu = (g_\mu - 2)/2$, may be explained by the presence of new weakly interacting particles with masses of a few 100 GeV. Particles of this kind can generally be directly produced at the LHC, and thus they may already be constrained by existing data. In this work, we investigate this connection between a_μ and the LHC in a model-independent approach, by introducing one or two new fields beyond the standard model with spin and weak isospin up to one. For each case, we identify the preferred parameter space for explaining the discrepancy of a_μ and derive bounds using data from LEP and the 8-TeV LHC run. Furthermore, we estimate how these limits could be improved with the 14-TeV LHC. We find that the 8-TeV results already rule out a subset of our simplified models, while almost all viable scenarios can be tested conclusively with 14-TeV data.

1 Introduction

The magnetic moment of the muon, $\vec{\mu}_\mu = \frac{e}{2m_\mu}(1+a_\mu)\vec{\sigma}$, is one of the most precisely measured quantities in particle physics and an important ingredient to electroweak precision tests [1].¹ It is well known that the experimental value for the anomalous contribution a_μ from the Brookhaven E821 experiment [2] differs from the standard model (SM) prediction by about three standard deviations. In particular, the analysis of [3] finds the discrepancy

$$\Delta a_\mu \equiv a_\mu^{\text{exp}} - a_\mu^{\text{th}} = (287 \pm 80) \times 10^{-11}. \quad (1)$$

There are three generic possible sources for this discrepancy: *(i)* the a_μ measurement itself, i.e. a statistical fluctuation or an overlooked systematic effect; *(ii)* uncertainties in the evaluation of non-perturbative hadronic corrections that enter in the SM prediction for a_μ ; or *(iii)* loop corrections from new particles beyond the SM. Concerning the first possibility, the experimental value will be cross-checked by the E989 experiment at Fermilab [4] and the planned $g-2$ /EDM experiment at J-PARC [5] in the near future. The hadronic corrections are difficult to evaluate, requiring input from experimental data, perturbative QCD, and non-perturbative hadronic models. However, several recent evaluations [6] yield results that all confirm a discrepancy of about 3σ or more.

In the presence of physics beyond the standard model (BSM), the leading one-loop contribution is parametrically of the order of $\delta a_\mu \sim \frac{g_{\text{NP}}^2}{16\pi^2} \frac{m_\mu^2}{M_{\text{NP}}^2}$, which can match the observed discrepancy for $\mathcal{O}(1)$ values of the couplings, g_{NP} , and $\mathcal{O}(100 \text{ GeV})$ values of the masses, M_{NP} , of the new particles. These ingredients can be satisfied by a large number of new-physics models, such as supersymmetry, extended gauge groups, extra dimensions, seesaw models, or extended Higgs sectors (see [3] and references therein).

In this article, rather than studying concrete BSM models and their impact on a_μ , we analyze minimal sets of new particles that can produce a one-loop correction of the required size. For definiteness, we consider one or two new fields with different spins and gauge-group representations. To allow a perturbative description for the a_μ correction, we focus on weakly coupled new physics, i.e. $|g_{\text{NP}}| \lesssim \sqrt{4\pi}$. We are interested in scenarios that can, at least in principle, be tested at collider experiments. Thus we do not consider very light superweakly coupled new particles, which can also successfully explain the a_μ discrepancy [7]. Instead, we restrict ourselves to new particles with weak-scale masses $M_{\text{NP}} \gtrsim 100 \text{ GeV}$. Particles of this kind are generically within reach of the LHC and may be additionally constrained by data from LEP.

The main goal of this paper is to establish a relationship between weak-scale BSM explanations for the discrepancy of the muon anomalous magnetic moment and direct searches for these particles at the LHC. After defining the overall framework and generic constraints in Section 2, we compute in Sections 3–5 the corrections to a_μ by adding one new field, two new mixed fermion fields, and two new fields with different spins to the SM, respectively. For each of these cases, we evaluate the viable parameter space that can explain the discrepancy in (1), given constraints from LEP and other lower-energy experiments. In Section 6, we

¹Here σ_i ($i = 1, 2, 3$) are the Pauli spin matrices.

explore how the viable new-physics scenarios can be probed at the LHC by recasting existing new-physics searches published by the ATLAS and CMS collaborations. While these experimental searches are generally not optimized for our purposes, they nevertheless lead to non-trivial constraints on new-physics explanations for the a_μ discrepancy. We also estimate how the reach could be extended with the full 14-TeV run of the LHC. In Section 7, we briefly comment on new-physics models where the a_μ correction is enhanced by $\tan\beta$, the ratio of the vacuum expectation values (vevs) of two Higgs doublets, which is not covered by the cases discussed in the previous sections. Finally, the conclusions are presented in Section 8.

2 Electroweak contributions

Electroweak SM contributions to a_μ are suppressed by $\mathcal{O}(m_\mu^2/M_W^2) = 10^{-6}$ with respect to QED contributions, due to the exchange of the massive gauge bosons.² At the one-loop level, they yield [1]

$$a_\mu^{\text{EW}} = \frac{G_F m_\mu^2}{8\sqrt{2}\pi^2} \left[\frac{5}{3} + \frac{1}{3}(1 - 4\sin^2\theta_W)^2 + \mathcal{O}\left(\frac{m_\mu^2}{M_{\text{EW}}^2}\right) \right] = 194.8 \times 10^{-11}, \quad (2)$$

with the Weinberg angle $\sin^2\theta_W \approx 0.2236$ and Fermi constant $G_F = 1.16638 \times 10^{-5} \text{ GeV}^{-2}$. Generically, new weakly-coupled particles with electroweak-scale masses M_{EW} will yield corrections of comparable size. Since the magnetic moment breaks parity, any contribution to a_μ involves a flip of the muon's chirality. This is typically achieved by a mass term, which breaks the chiral symmetry of the underlying theory. New electroweak contributions to a_μ are therefore expected to exhibit the same suppression $\mathcal{O}(m_\mu^2/M_{\text{EW}}^2)$ as in the SM.

We aim at performing a model-independent analysis of contributions to a_μ from new particles around the electroweak scale. We consider all possible one-loop contributions of fields with spin 0, 1/2 and 1 that are singlets, doublets or triplets under the gauge group SU(2) of weak interactions, and with integer electric charges. In Table 1, we introduce the corresponding notation and give examples of models which incorporate such new particles. Their contributions to a_μ can be classified with respect to the fields occurring in the loop:

1. One new field and a SM lepton, W , Z or Higgs boson (Figure 2).
2. Two new mixing fermions and a W , Z or Higgs boson (Figure 1, left).
3. Two new fields with different spins (Figure 4).

We will discuss these three categories one by one in the following sections. Contributions with two mixing fermions (2.) always imply contributions with one new fermion (1.). All other two-field contributions (3.) may imply one-field contributions (1.). The latter, however, can be strongly constrained by measurements of other observables (as will be discussed in

²The contributions from Higgs bosons receive an additional suppression by m_μ^2/M_H^2 from the muon Yukawa coupling.

Vector bosons	V^0, V^\pm, V_A	Z', W' , left-right symmetric electroweak sector (V_A)
Scalar bosons	$\phi^0, \phi^\pm, \phi_D, \phi_A, \phi_T$	extended Higgs sectors, seesaw type II (ϕ_T)
Fermions	$\psi^0, \psi^\pm, \psi_D, \psi_A, \psi_T$	composite fermions, seesaw type III (ϕ_A)

Table 1: New fields considered in this work, their electroweak properties and examples for models in which they appear. $0, \pm$: neutral, charged weak singlets. D : weak doublet with hypercharge $\pm 1/2$. A, T : weak triplets with hypercharge $0, -1$.

the following subsections) or entirely prohibited due to a discrete symmetry.³ Diagrams with two new fields in the loop can therefore become the dominant contribution to Δa_μ . In addition to contributions from new particles in the loop, the electroweak SM contributions to a_μ can be modified by the mixing of new fermions with SM leptons through corrections to the lepton gauge couplings and Yukawa couplings. In models that incorporate at least two scalar fields with vevs v_1 and v_2 , additional contributions enhanced by $\tan \beta = v_1/v_2$ occur. These effects will be discussed separately in Section 7.

2.1 Constraints from LEP observables

New electroweak contributions to a_μ are generally constrained by precision observables and direct searches at LEP. In this section, we study generic constraints on the masses and couplings of new particles that apply to all the cases discussed in the following sections. We focus on robust constraints with a model-independent connection to a_μ . Along those lines, processes involving couplings to quarks are not taken into account, since they can easily be circumvented in hadrophobic models.

Direct mass constraints on new particles can be obtained from LEP II searches for pair production via gauge interactions with a Z boson or photon, namely $e^+e^- \rightarrow Z/\gamma \rightarrow XX$. Assuming one dominant decay mode (new bosons decay mainly into leptons, new fermions decay via electroweak currents through mixing with SM leptons), mass constraints are independent from the couplings to fermions. The non-observation of new vector bosons, scalars and fermions at center-of-mass (CM) energies around $\sqrt{s} \approx 200$ GeV yields a general mass bound of $M \gtrsim 100$ GeV (see for instance the listings for Higgs bosons, heavy charged-lepton searches, and other lepton searches in [1]). These constraints do not apply to SM gauge singlets, which cannot be produced through electroweak interactions.⁴

The exchange of a new heavy scalar or gauge boson in $e^+e^- \rightarrow \ell^+\ell^-$ processes leads to four-lepton contact interactions, which are strongly constrained by LEP measurements. Details will be discussed in Section 3. Besides the resonant production of one new particle, similar constraints also apply to couplings of two new particles to a lepton, which generate four-lepton interactions at one-loop level. Due to the loop suppression, the bounds are

³A prominent example for such a symmetry is R parity in models with supersymmetry.

⁴Since we assume that new scalar fields do not acquire a vev, associated production with a Z boson is prohibited.

generally weaker than for one new particle, but important if new particles couple strongly to leptons. One-loop effects on four-lepton interactions will be discussed in detail in Section 5, analytic results are given in Appendix B. We emphasize that our results are model-independent and can thus be of general use to constrain the couplings of two new particles to leptons from LEP measurements.

Strong constraints on new particles in weak multiplets arise from the “oblique” parameters S and T [20]. The T parameter is sensitive to weak isospin breaking through mass splitting among the multiplet constituents. To prevent large contributions to T , we require (approximate) mass degeneracy for the components of SU(2) doublets or triplets. The S parameter probes different isospin three-components T_3 of left- and right-chiral fermions, $S \sim [T_3(\psi_L) - T_3(\psi_R)]^2$. To avoid such effects, we impose vector-like couplings of new fermions to gauge bosons. This simultaneously ensures the cancellation of axial-vector gauge anomalies.

In summary, we assume the following properties of new particles in our analysis:

- Particles with electroweak quantum numbers are heavier than 100 GeV.
- Constituents of weak multiplets are degenerate in mass.
- Couplings involving new particles are real and perturbative, *i.e.* smaller than $\sqrt{4\pi}$.
- New fermions have vector-like electroweak couplings.
- All interactions involving leptons are minimally flavor-violating.

By limiting ourselves to couplings without an imaginary part, we circumvent potential (model-dependent) constraints from the electric dipole moment of the electron [9]. The assumption of minimal flavor violation (MFV) is motivated by strong constraints from the process $\mu \rightarrow e\gamma$ and from the smallness of the muon mass. These constraints and their relation to a_μ will be discussed in detail in the following Section 2.2.

2.2 Constraints from $\mathcal{B}(\mu \rightarrow e\gamma)$ and the muon mass

The flavor-conserving anomalous magnetic moment a_μ is tightly connected to the flavor-violating process $\mu \rightarrow e\gamma$. In the framework of an effective theory, new-physics contributions to both quantities are described by dimension-six operators with the same gauge and Lorentz structure [10],

$$\begin{aligned} O_{a_\mu}^1 &= g' y_\mu H^\dagger \overline{\mu_R} \sigma^{\mu\nu} \mu_L B_{\mu\nu}, & O_{\mu e}^1 &= g' y_\mu H^\dagger \overline{e_R} \sigma^{\mu\nu} \Delta_{\mu e} \mu_L B_{\mu\nu}, \\ O_{a_\mu}^2 &= g y_\mu H^\dagger \overline{\mu_R} \sigma^{\mu\nu} \tau^a \mu_L W_{\mu\nu}^a, & O_{\mu e}^2 &= g y_\mu H^\dagger \overline{e_R} \sigma^{\mu\nu} \Delta_{\mu e} \tau^a \mu_L W_{\mu\nu}^a, \end{aligned} \quad (3)$$

where y_μ is the muon Yukawa coupling, H is the SM Higgs doublet with vev $v = 246$ GeV, and $B_{\mu\nu}$ and $W_{\mu\nu}^a$ are the U(1) and SU(2) gauge fields before electroweak symmetry breaking with the corresponding gauge couplings g' and g . The labels L, R on the fermion fields denote left- and right-chiral states, respectively, while $\overline{\psi_{L,R}}$ denote anti-fermions with the

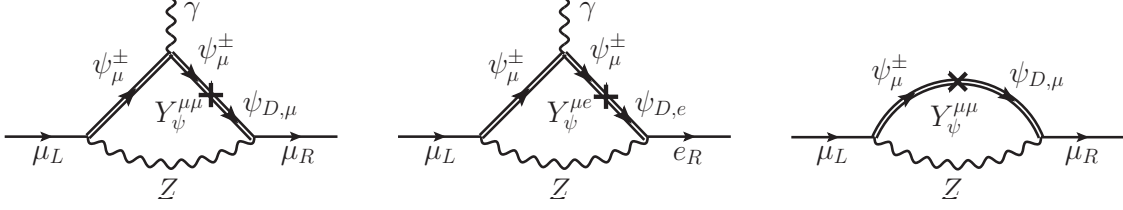


Figure 1: Contributions of new heavy leptons to a_μ , $\mathcal{B}(\mu \rightarrow e\gamma)$, and m_μ (from left to right). Shown are representative diagrams for the case of weak charged-singlet (ψ^\pm) and doublet (ψ_D) leptons. The indices e and μ denote positions 1 and 2 in flavor space, respectively.

same chirality, i.e. opposite helicity. The amount of flavor violation is parametrized by $\Delta_{\mu e}$. The branching ratio of $\mu \rightarrow e\gamma$ normalized to $\mu \rightarrow e\nu_\mu\bar{\nu}_e$ is given by [10]

$$\mathcal{B}(\mu \rightarrow e\gamma) = 384 \pi^2 e^2 \frac{v^4}{\Lambda_{\text{FV}}^4} |\Delta_{\mu e}|^2 |C_{\mu e}^1 - C_{\mu e}^2|^2 \approx 6.34 \times 10^{-7} \left(\frac{1 \text{ TeV}^4}{\Lambda_{\text{FV}}^4} \right) |\Delta_{\mu e}|^2, \quad (4)$$

where $C_{\mu e}^i \approx \mathcal{O}(1)$ are Wilson coefficients and $\Lambda_{\text{FV}} \gg v$ denotes the scale at which lepton flavor violation occurs explicitly through new degrees of freedom. The current experimental bound $\mathcal{B}(\mu \rightarrow e\gamma) < 2.4 \times 10^{-12}$ [1] imposes strong constraints on $|\Delta_{\mu e}|/\Lambda_{\text{FV}}^2$. This implies that contributions to a_μ from a scale $\Lambda \approx \Lambda_{\text{FV}} \lesssim 1 \text{ TeV}$ (necessary to explain the discrepancy Δa_μ) are ruled out, unless a protection mechanism is at work that suppresses the flavor violation $\Delta_{\mu e}$.

The lepton sector of the SM has an accidental approximate flavor symmetry $\mathcal{G}_F = SU(3)_L \times SU(3)_e$, under which weak doublet and charged singlet leptons transform as $(3, 1)$ and $(1, 3)$ representations, respectively. The flavor symmetry is broken only by the charged-lepton and neutrino Yukawa couplings \mathbf{Y}_ℓ and \mathbf{Y}_ν , a pattern referred to as minimal flavor violation.

The presence of new vector leptons generally introduces new sources of lepton flavor violation through their mass term \mathbf{M}_ψ and Yukawa coupling \mathbf{Y}_ψ to SM leptons or other vector leptons. We extend the principle of MFV to vector leptons by making the following demands. Vector leptons transform under \mathcal{G}_F as either $(3, 1)$ or $(1, 3)$ representations, which implies three flavor copies of each new vector lepton. Furthermore, \mathbf{M}_ψ and \mathbf{Y}_ψ must transform under \mathcal{G}_F as appropriate combinations of $\mathbf{Y}_\ell = (3, \bar{3})$ and $\mathbf{Y}_\nu = (3, 1)$. This principle applies accordingly to new vector bosons with gauge couplings \mathbf{G}_V or scalars with couplings \mathbf{G}_ϕ . In the eigenbasis of weak interactions, the masses and couplings of new particles thus respect the following pattern in flavor space,

$$\begin{aligned} \mathbf{M}_\psi &= m_\psi (\mathbf{1} + c_M \Delta'_\psi), & \mathbf{Y}_\psi &= y_\psi \mathbf{Y}_\ell (1 + c_\psi \Delta_\psi) \quad \text{or} \quad y_\psi (\mathbf{1} + c'_\psi \Delta'_\psi), \\ \mathbf{G}_V &= g_V (\mathbf{1} + c_V \Delta_V), & \mathbf{G}_\phi &= g_\phi \mathbf{Y}_\ell (1 + c_\phi \Delta_\phi) \quad \text{or} \quad g_\phi (\mathbf{1} + c'_\phi \Delta'_\phi), \end{aligned} \quad (5)$$

where y_ψ , g_V , g_ϕ , c_i and c'_i are arbitrary coefficients of $\mathcal{O}(1)$ and m_ψ sets the scale for the masses of vector leptons. For our purposes, $c_M \Delta'_\psi$ and $c_V \Delta_V$ can be neglected, yielding flavor-universal masses $\mathbf{M}_\psi = m_\psi \times \mathbf{1}$ and gauge couplings $\mathbf{G}_V = g_V \times \mathbf{1}$. Flavor violation is

potentially induced by the matrices Δ_i , which are combinations of \mathbf{Y}_ℓ and \mathbf{Y}_ν of $\mathcal{O}(\mathbf{Y}_{\ell,\nu}^2)$ and higher. The exact form of Δ_i , as well as the transformation properties of \mathbf{Y}_ψ and \mathbf{G}_ϕ under the flavor group, depend on the representation of the (vector) leptons. In particular, the magnitude of the mixing between new vector leptons is determined by $\mathbf{Y}_\psi \sim \mathbf{Y}_\ell$ ($\mathbf{Y}_\psi \sim \mathbf{1}$), if they are in different (in the same) representations of \mathcal{G}_F . The consequences on effects in a_μ will be discussed in Section 4.

Under these conditions, contributions to $\mathcal{B}(\mu \rightarrow e\gamma)$ from vector leptons are suppressed by neutrino mass splittings (encoded in Δ) as in the SM, but effects in flavor-conserving observables such as a_μ can be sizeable. In Figure 1, we illustrate contributions of vector leptons to a_μ (left) and $\mathcal{B}(\mu \rightarrow e\gamma)$ (center) for the case of a weak singlet $\psi^\pm = (3, 1)$ and a doublet $\psi_D = (1, 3)$. In the mass eigenbasis of the charged leptons, the Yukawa couplings are given by $Y_\psi^{\mu\mu} = y_\psi y_\mu$ and $Y_\psi^{\mu e} = \Delta_{\mu e} y_\mu$, where $\Delta_{\mu e}$ is proportional to the neutrino mass splittings.

Minimal flavor violation also protects the SM lepton masses from overly large quantum corrections induced by vector leptons. In general, the Yukawa mixing \mathbf{Y}_ψ between vector leptons in different flavor representations induces potentially large contributions to the lepton masses, $\mathbf{M}_\ell = (\mathbf{Y}_\ell + \mathbf{Y}_\psi L) v/\sqrt{2}$, where L is a loop factor of $\mathcal{O}(1/(4\pi))$. These effects are illustrated in Figure 1, right. Within the framework of MFV, mass corrections are proportional to the lepton Yukawa coupling, yielding

$$\mathbf{M}_\ell = \mathbf{Y}_\ell(1 + y_\psi L) v/\sqrt{2}. \quad (6)$$

Perturbativity imposes an upper bound of $|y_\psi| \lesssim \sqrt{4\pi}/y_\tau \approx 3.5 \times 10^2$. For effects in the muon sector, the relevant Yukawa coupling is thus confined to $|Y_\psi^{\mu\mu}| = |y_\psi y_\mu| \lesssim 0.2$. If vector leptons are in the same flavor representation, their mixing Y_ψ is unconstrained by MFV. In this case, the muon mass is protected by the suppressed mixing of vector leptons with SM leptons, which will be discussed in Section 4.

2.3 Calculational techniques and tools

The calculation of our new electroweak contributions to a_μ is performed in a semi-automated way. We generate the one-loop amplitudes for the process $\mu \rightarrow \mu\gamma$ in the unitary gauge using the FEYNARTS package [11], supplemented by the Feynman rules for the new particles. The calculation of the contributions to a_μ is greatly simplified by applying a projection technique that singles out the magnetic form factor [12]. Subsequently, amplitudes are evaluated for zero momentum transfer and expanded up to leading order, $\mathcal{O}(m_\mu^2)$, in the small muon mass (or, equivalently, the muon Yukawa coupling). This procedure, as well as the reduction of the loop integrals, has been performed with two independent computer programs, one of which is based on FEYNALC [13], while the other is a private code. We thereby have obtained a cross check of all analytic results.

By assuming that the correction to a_μ in a given new-physics scenario can explain the observed discrepancy in (1), we obtain constraints on the parameter space of particle masses and couplings. In some cases, the correction turns out to have the wrong sign or is generically too small. As described in the next sections, we still find a number of scenarios that provide

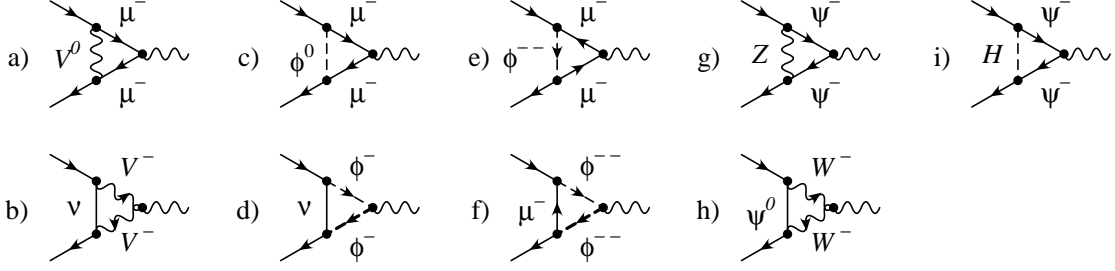


Figure 2: Electroweak contributions to a_μ with one new particle in the vertex loop.

a successful explanation for the discrepancy. We then analyze the production mechanism and typical decay signatures of the new particles at the LHC. For this purpose, we do not assume any additional particle content and couplings besides those appearing in the a_μ loop corrections or required by gauge invariance. Cross sections and event rates are computed at the parton level using the program CALCHEP [14]. We then aim at setting bounds on the allowed parameter space from LHC data by recasting existing BSM searches of the ATLAS and CMS collaborations.

3 One new field

This section discusses scenarios where a single new field (that couples to muons) at a time is added to the SM. For all fields listed in Table 1, we analyze their contributions to a_μ and potential constraints from LEP observables. Subsequently, we identify the parameter space that can explain the discrepancy Δa_μ . Analytic results for the contributions to a_μ are summarized in Table 3 in Appendix A.

Neutral vector boson (V^0): A massive neutral vector boson with the effective couplings to leptons of the form

$$\mathcal{L} \supset g_L \bar{\ell}_L \gamma^\mu \ell_L V_\mu^0 + g_R \bar{\ell}_R \gamma^\mu \ell_R V_\mu^0 \quad (7)$$

can contribute to a_μ through the diagram in Figure 2 (a). The correction δa_μ becomes maximal for $g_L = g_R \equiv g_V$, for fixed $\sqrt{g_L^2 + g_R^2}$, in which case the discrepancy in (1) can be explained for

$$0.0047 \text{ GeV}^{-1} < g_V/M_V < 0.0062 \text{ GeV}^{-1} \quad (8)$$

at the one-sigma level. As long as V^0 does not mix with the Z boson, constraints from Z -pole precision observables at LEP can be evaded. However, assuming MFV, the interaction (7) generates $ee\mu\mu$ and $eeee$ contact interactions, which have been strongly constrained by the LEP experiments at CM energies of $\sqrt{s} \approx 130 - 200 \text{ GeV}$. For $M_V > \sqrt{s}$, the limit from [15] on the scale Λ of the $ee\mu\mu$ operator can be translated into the 95% C.L. upper bound

$$g_V/M_V = \sqrt{4\pi}/\Lambda < 0.00022 \text{ GeV}^{-1}, \quad M_V > 200 \text{ GeV}. \quad (9)$$

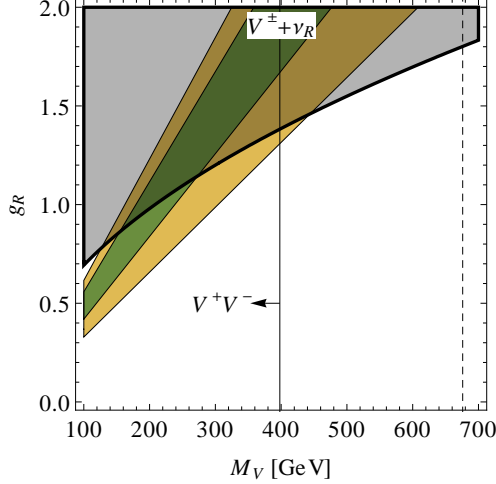


Figure 3: Contribution to a_μ from a charged vector boson V^\pm and a light right-handed neutrino ν_R in the vertex loop. The parameter space to explain Δa_μ at the 1σ (2σ) level is displayed in green (yellow). The 95% C.L. region excluded by $eell$ contact interaction searches at LEP is shaded gray. Lower mass bounds at 95% C.L. from direct searches at the 8-TeV LHC and projections for 14 TeV (see Section 6) are displayed as plain and dashed black lines, respectively.

For $M_V < \sqrt{s}$, neutral vector bosons can be resonantly produced via $e^+e^- \rightarrow V^0\gamma \rightarrow \ell^+\ell^-\gamma$, where γ is a soft or hard photon. The cross section for the production of a narrow resonance R with a total width Γ_R is proportional to

$$\sigma(e^+e^- \rightarrow R\gamma \rightarrow \ell^+\ell^-\gamma) \propto \frac{2j+1}{\Gamma_R} \Gamma(R \rightarrow e^+e^-) \Gamma(R \rightarrow \ell^+\ell^-), \quad (10)$$

with $j = 1(0)$ for a vector (scalar) resonance. The partial decay widths of vectors and scalars into leptons are given by $\Gamma(V \rightarrow \ell^+\ell^-) = g_\ell^2 M_V / (24\pi)$ and $\Gamma(\phi \rightarrow \ell^+\ell^-) = g_\ell^2 M_\phi / (16\pi)$, respectively. At LEP, resonance searches for scalar neutralinos with R -parity violating couplings λ have been performed at CM energies in the range of $\sqrt{s} = 130 \dots 189$ GeV [16]. For a decay width $\Gamma_{\tilde{\nu}} \leq 1$ GeV, the couplings to leptons are constrained to $\lambda < 0.02 \dots 0.08$ at the 95% C.L., depending on the neutralino mass $M_{\tilde{\nu}}$, in the mass range $100 \text{ GeV} < M_{\tilde{\nu}} < 200 \text{ GeV}$. Interpreting the bounds on λ for vector bosons and fixing the total decay width to $\Gamma_V = 1$ GeV,⁵ yields the conservative 95% C.L. upper bound

$$g_V/M_V < 0.08 \times \sqrt[4]{3/4}/M_V \lesssim 0.00075 \text{ GeV}^{-1}, \quad 100 \text{ GeV} < M_V < 200 \text{ GeV}. \quad (11)$$

The bounds from contact interactions (9) and resonance searches (11) at LEP therefore rule out sizeable contributions to a_μ from neutral vector bosons. For the same reasons, any $SU(2)$ multiplet of vector bosons containing a neutral vector field is excluded.

Charged vector boson (V^\pm): A charged vector boson can contribute to a_μ through the diagram in Figure 2 (b). Since limits from electroweak precision tests are stronger for a coupling of V^\pm to left-handed SM fermions than to right-handed fermions (due to interference with the W boson), the latter case is considered here,

$$\mathcal{L} \supset g_R \bar{\ell}_R \gamma^\mu \nu_R V_\mu^- + \text{h.c.} \quad (12)$$

⁵For larger decay widths, the bound on g_V is mildly relaxed. For instance, for $\Gamma_V = 10$ GeV, resonance searches yield $g_V < 0.14$, which is still below the range required to explain Δa_μ .

We do not speculate about the nature of the right-handed neutrino and assume it to be light ($M_{\nu_R} \ll M_{\text{EW}}$),⁶ but still heavy enough ($M_{\nu_R} \gtrsim 100$ MeV) to evade potential bounds from muon decay and astrophysics. In this range, the contribution to a_μ is well approximated by $M_{\nu_R} = 0$, and the discrepancy (1) can a priori be explained at the one-sigma level for

$$0.0042 \text{ GeV}^{-1} < g_R/M_V < 0.0056 \text{ GeV}^{-1}. \quad (13)$$

The corresponding parameter space is displayed in Figure 3. Constraints on V^\pm contributions to a_μ are derived from bounds on four-lepton contact interactions at LEP. The leading effect occurs at the one-loop level through the box diagram in Figure 5 (c). This effect yields the 95% C.L. bound $g_R^2/M_V < 0.0048 \text{ GeV}^{-1}$, which excludes the parts of the parameter space corresponding to the gray region in Figure 3. One-loop four-lepton interactions will be discussed in detail in Section 5, where they play a crucial role in constraining couplings of SM leptons to two new fields with different spins.

Scalar doublet (ϕ_D): For a scalar doublet, one can write down lepton couplings similar to the Yukawa couplings of the SM Higgs boson,

$$\mathcal{L} \supset -Y \overline{L}_L \phi_D \ell_R + \text{h.c.}, \quad \phi_D = \begin{pmatrix} \phi_D^+ \\ \phi_D^0 \end{pmatrix}, \quad (14)$$

where L_L is the left-handed SM lepton doublet and $\phi_D^{+,0}$ are the charged and neutral (complex) components of ϕ_D , respectively. It is assumed that ϕ_D does not have a vev that would contribute to fermion masses. The scalar doublet can contribute to a_μ through the diagrams Figure 2 (c,d). It turns out that ϕ_D can successfully accommodate Δa_μ for

$$0.0076 \text{ GeV}^{-1} < Y/M_\phi < 0.0102 \text{ GeV}^{-1} \quad (15)$$

at the one-sigma level. As for a neutral vector boson, the exchange of a neutral scalar in e^+e^- collisions generates four-lepton contact interactions for $M_\phi > \sqrt{s}$. Direct constraints on scalar four-fermion contact interactions from LEP do not exist. Still, the bounds on $eeee$ vector interactions can be interpreted as bounds on scalar interactions by using the Fierz identity

$$(\overline{e}_R e_L)(\overline{e}_L e_R) + (\overline{e}_L e_R)(\overline{e}_R e_L) = \frac{1}{2} [(\overline{e}_L \gamma_\mu e_L)(\overline{e}_R \gamma_\mu e_R) + (\overline{e}_R \gamma_\mu e_R)(\overline{e}_L \gamma_\mu e_L)]. \quad (16)$$

The limits from [15] on the scale Λ_{LR} of the LR (and RL) four-electron vector operator thus translate into the 95% C.L. limit

$$Y/M_\phi = \sqrt{2\pi}/\Lambda_{\text{LR}} < 0.00025 \text{ GeV}^{-1}, \quad M_\phi > 200 \text{ GeV}. \quad (17)$$

For $M_\phi < \sqrt{s}$, the LEP searches for neutralino resonances discussed around (10) apply directly to neutral scalars. They lead to the 95% C.L. upper bound

$$Y/M_\phi < 0.08/M_\phi \lesssim 0.0008 \text{ GeV}^{-1}, \quad 100 \text{ GeV} < M_\phi < 200 \text{ GeV}. \quad (18)$$

By comparing the bounds from (18) and (17) with (15), it is evident that a scalar doublet as an explanation of Δa_μ is ruled out by LEP searches for neutral scalars.

⁶The case of weak-singlet neutrinos $\nu_R = \psi^0$ with $M_{\psi^0} \approx M_{\text{EW}}$ will be discussed in Section 5.

Scalar triplet (ϕ_T): A scalar triplet ϕ_T with hypercharge -1 can couple to muons through the interaction

$$\mathcal{L} \supset -\frac{Y}{2} \bar{L}_L \phi_T i \sigma_2 L_L^c + \text{h.c.}, \quad \phi_T = \begin{pmatrix} \phi_T^-/\sqrt{2} & \phi_T^0 \\ \phi_T^{--} & -\phi_T^-/\sqrt{2} \end{pmatrix}, \quad (19)$$

where σ_2 is the second Pauli matrix. The correction δa_μ , corresponding to the diagrams in Figure 2 (c-f), is always negative and thus cannot explain the observed discrepancy Δa_μ .

Vector-like fermions ($\psi^0, \psi^\pm, \psi_D, \psi_A, \psi_T$): New fermions with vector-like mass terms can couple to the SM leptons through Yukawa couplings involving the SM Higgs doublet H . We consider the following cases:

- A neutral SU(2) singlet ψ^0 ;
- A charged SU(2) singlet ψ^\pm ;
- An SU(2) doublet ψ_D with the same quantum numbers as the left-handed SM lepton doublet;
- An SU(2) triplet ψ_A with hypercharge 0 (*i.e.* in the adjoint representation) and Majorana mass term;
- An SU(2) triplet ψ_T with hypercharge -1 .

The relevant Yukawa couplings for these five cases are given by

$$\mathcal{L} \supset -Y \bar{L}_L \tilde{H} \psi_R^0 + \text{h.c.}, \quad (20)$$

$$\mathcal{L} \supset -Y \bar{L}_L H \psi_R^- + \text{h.c.}, \quad (21)$$

$$\mathcal{L} \supset -Y \bar{\psi}_{D,L} H \ell_R + \text{h.c.}, \quad \psi_D = \begin{pmatrix} \psi_D^0 \\ \psi_D^- \end{pmatrix}, \quad (22)$$

$$\mathcal{L} \supset -Y \tilde{H}^\dagger \bar{\psi}_{A,R} L_L + \text{h.c.}, \quad \psi_A = \begin{pmatrix} \psi_A^0/\sqrt{2} & \psi_A^+ \\ \psi_A^- & -\psi_A^0/\sqrt{2} \end{pmatrix}, \quad (23)$$

$$\mathcal{L} \supset -Y H^\dagger \bar{\psi}_{T,R} L_L + \text{h.c.}, \quad \psi_T = \begin{pmatrix} \psi_T^-/\sqrt{2} & \psi_T^0 \\ \psi_T^{--} & -\psi_T^-/\sqrt{2} \end{pmatrix}, \quad (24)$$

where $\tilde{H} = i\sigma_2 H^*$. After electroweak symmetry breaking, when H acquires a vev $\langle H \rangle = (0, v/\sqrt{2})^\top$, these interactions lead to mixing between the vector-like fermions and the SM charged leptons or neutrinos, which can be expressed in terms of the mixing parameter $\epsilon = Yv/M_\psi$. The mixing affects the electroweak couplings of SM leptons by corrections of $\mathcal{O}(\epsilon^2)$ and induces new gauge and Yukawa interactions of a vector lepton with a SM boson and a SM lepton of $\mathcal{O}(\epsilon)$. The former effect modifies the size of the SM electroweak contributions to a_μ , whereas the new couplings lead to additional contributions to a_μ from the diagrams in Figure 2 (g), (h) and/or (i). The corrections to a_μ are of $\mathcal{O}(\epsilon^2)$ in either

case. Details on vector lepton mixing and the resulting electroweak couplings in the context of a_μ can be found, for instance, in [17, 18].

The analytic results for effects of mixing vector leptons on a_μ are listed in Table 3 in Appendix A. For the neutral singlet ψ^0 and the triplets ψ_A , ψ_T , the correction δa_μ is negative. For the charged singlet ψ^\pm , δa_μ is positive for $M_\psi \gtrsim 250$ GeV, but too small to explain the observed discrepancy with perturbative couplings $|Y| < \sqrt{4\pi}$. The contribution of the doublet ψ_D can a priori accommodate Δa_μ for strong mixing $|\epsilon| \gtrsim 1.2$ and perturbative couplings in the mass range $100 \text{ GeV} < M_\psi < 500 \text{ GeV}$. However, the mixing between SM leptons and heavy vector leptons is strongly constrained by Z -pole precision measurements at LEP. Assuming flavor-universal couplings, a global fit to LEP data leads to the bound $|\epsilon| \lesssim 0.03$ for mixing with a vector lepton doublet [19], clearly ruling out any significant contribution to a_μ .

4 Two new mixed fermion fields

In the previous Section 3, we have seen that effects on a_μ from a single species of vector-like fermions are either negative or too small to explain the discrepancy Δa_μ in (1). However, larger corrections may in principle be obtained from the simultaneous presence of two types of vector leptons that mix with each other [17, 18]. Possible combinations in accord with weak quantum numbers are a weak doublet ψ_D with either a neutral singlet ψ^0 , a charged singlet ψ^\pm , a weak adjoint triplet ψ_A , or a triplet ψ_T with hypercharge -1 .

In addition to the mixing with SM fermions in (20)–(24), vector leptons with different weak quantum numbers mix through Yukawa couplings to the SM Higgs boson. The Lagrangian describing the mixing of a doublet with a singlet or a triplet reads

$$\mathcal{L}_{DS}^{\text{mix}} = -Y_{DS} \overline{\psi_{D,L}} H \psi_R^- - Y_{SD} \overline{\psi_L^-} H^\dagger \psi_{D,R} + \text{h.c.} \quad (25)$$

$$\mathcal{L}_{DN}^{\text{mix}} = -Y_{DN} \overline{\psi_{D,L}} \tilde{H} \psi_R^0 - Y_{ND} \overline{\psi_L^0} \tilde{H}^\dagger \psi_{D,R} + \text{h.c.} \quad (26)$$

$$\mathcal{L}_{DA}^{\text{mix}} = -Y_{DA} \overline{\psi_{D,L}} \psi_{A,R} \tilde{H} - Y_{AD} \tilde{H}^\dagger \overline{\psi_{A,L}} \psi_{D,R} + \text{h.c.} \quad (27)$$

$$\mathcal{L}_{DT}^{\text{mix}} = -Y_{DT} \overline{\psi_{D,L}} \psi_{T,R} H - Y_{TD} H^\dagger \overline{\psi_{T,L}} \psi_{D,R} + \text{h.c.} \quad (28)$$

The required chirality flip in a_μ can thus proceed through the mixing between heavy leptons ($\sim Y_{12}v$) rather than muons ($\sim y_\mu v$), as illustrated in Figure 1, left.⁷ Contributions to a_μ from mixed vector leptons are thus enhanced by a factor of Y_{12}/y_μ with respect to contributions from single vector leptons. The complete analytic results for a_μ in the scenarios $\psi_D + \psi^\pm$, $\psi_D + \psi^0$, $\psi_D + \psi_A$, and $\psi_D + \psi_T$ are listed in Appendix A in (53) and (54); the corresponding couplings are defined in Tables 5 and 6. They are obtained by diagonalizing the mass matrices with mixing leptons ℓ and ψ_1 or ψ_2 to first order in the parameters $\epsilon_i = Y_i v / M_i$ (the mixing of SM leptons ℓ with vector leptons ψ_i) and $\omega_{12} = Y_{12} v / (M_1 - M_2)$ (the mixing among vector leptons ψ_1 and ψ_2). We thereby retain the leading effects on a_μ up to $\mathcal{O}(\epsilon^2 \omega)$ for moderate mixing $|\epsilon_{1,2}|, |\omega_{12}| \lesssim 1$. The overall structure of a_μ can be expressed

⁷ Y_{12} stands for either of the Yukawa couplings Y_{SD} , Y_{DS} , etc. inducing vector lepton mixing.

as the sum of contributions from single vector leptons and contributions from mixed vector leptons,

$$a_\mu(\psi_1, \psi_2) = m_\mu^2 \epsilon_1^2 F_1(M_1^2) + m_\mu^2 \epsilon_2^2 F_2(M_2^2) + m_\mu M_{1,2} \epsilon_1 \epsilon_2 \omega_{12} G(M_1^2, M_2^2), \quad (29)$$

where F and G are functions of the vector lepton masses M_1 , M_2 and their couplings to SM bosons. Due to the enhancement of contributions with vector lepton mixing, the main effect on a_μ is to a good approximation given by the third term in (29). Without any further assumptions, the discrepancy Δa_μ can be accommodated for $M_{1,2} > 100$ GeV and couplings of $\mathcal{O}(0.1\dots 1)$ in all scenarios.

The measurements of electroweak precision observables at LEP constrain the mixing with SM leptons to $|\epsilon_{S,D,T}| \lesssim 0.03$ and $|\epsilon_{N,A}| \lesssim 0.05$ for flavor-universal couplings [19]. In the framework of MFV, additional constraints on the couplings depend on the flavor representation (see Section 2.2). We consider two MFV scenarios, which result in the suppression of either the mixing with SM leptons ϵ_i or the mixing among vector leptons Y_{12} . Here we discuss them exemplarily for the case of vector singlet–doublet mixing.

1. Vector leptons are in the same representation as the SM leptons they mix with, i.e. $\psi_D = (1, 3)$ and $\psi^\pm = (3, 1)$.⁸ The couplings to SM leptons from (21) and (22) are thus flavor-conserving and the mixing parameter ϵ is unconstrained by MFV. The (flavor-breaking) mixing between ψ_D and ψ^\pm is proportional to the muon Yukawa coupling, $Y_{12} = y_{12} y_\mu$ ($12 = SD, DS$). Including LEP constraints and requiring perturbativity, the couplings are limited to $|\epsilon_{S,D}| \lesssim 0.03$ and $|Y_{12}| \lesssim 0.2$.
2. Vector leptons are in the same representation, $\psi_D, \psi^\pm = (1, 3)$, or $\psi_D, \psi^\pm = (3, 1)$. In this case, only the coupling between ψ^\pm (ψ_D) and SM leptons breaks the flavor symmetry, yielding the bound $|\epsilon_{S(D)}| M_{S(D)} / v = |Y_{S(D)}| y_\mu \lesssim 0.2$. Since LEP limits are stronger than the MFV suppression in the mass range up to $M_{S,D} \sim 1.6$ TeV, the couplings in either case are eventually limited to $|\epsilon_{S,D}| \lesssim 0.03$. The mixing among vector fermions is unconstrained by the requirement of MFV, yielding $|Y_{12}| \lesssim \sqrt{4\pi}$.

In scenario 1, the maximal contributions to a_μ are of $\mathcal{O}(10^{-10})$, which is one order of magnitude too small to accommodate Δa_μ in (1) within two sigma. In scenario 2, the discrepancy may a priori be explained by vector leptons around M_{EW} with sizeable mixing $Y_{12} \gtrsim 0.5$ in all four scenarios.

However, strong constraints on vector lepton mixing arise from the anomalous magnetic moment of the electron a_e . The discrepancy between the precise measurement and SM prediction has been found to be [21]

$$\Delta a_e \equiv a_e^{\text{exp}} - a_e^{\text{th}} = (-1.06 \pm 0.82) \times 10^{-12}. \quad (30)$$

Within the framework of MFV, effects of mixing vector leptons on a_μ and a_e are tightly related. The dominant contribution $\delta a_\mu \sim m_\mu M_\psi Y_{12}$ with a flavor-universal mixing Y_{12}

⁸In scenarios with vector lepton triplets, these transform in the same way as vector lepton singlets under the flavor group.

(corresponding to scenario 2) implies a contribution to a_e given by

$$\delta a_e = \frac{m_e}{m_\mu} \times \delta a_\mu = +1.4 \times 10^{-11} \quad \text{for} \quad \delta a_\mu = \Delta a_\mu. \quad (31)$$

Any sizeable contribution to a_μ that could explain the discrepancy Δa_μ in (1) is therefore clearly ruled out by Δa_e in (30). The maximal contribution to a_μ in agreement with Δa_e in its two-sigma range is $\delta a_\mu = 1.2 \times 10^{-10}$, which is of about the same magnitude as in scenario 1.

Beyond MFV (and beyond our working hypothesis), large vector lepton mixing is in general prohibited by $\mu \rightarrow e\gamma$, as we discussed in Section 2.2. The only way to circumvent this strong constraint is to suppress the coupling of vector leptons to electrons, $Y\bar{\psi}eH$. In this case, Δa_μ can be explained with mixing vector fermions even beyond the TeV mass range. In the scenarios $\psi_D + \psi^\pm$, $\psi_D + \psi_A$ and $\psi_D + \psi_T$, the dominant contributions to a_μ decouple as $Y_D Y_i Y_{12}/(M_D M_i)$, $i = S, A, T$, for $M_\psi \gg M_{\text{EW}}$. However, since LEP constraints on $Y_{1,2} = \epsilon_{1,2} M_{1,2}/v$ weaken as $M_{1,2}$ become large, the *maximal* contribution to a_μ is asymptotically constant. In the scenario $\psi_D + \psi^0$, the dominant contribution due to vector fermion mixing decouples as $Y_N Y_D Y_{12}/M_D^2$ for $M_D \gg M_{\text{EW}}$ and as $Y_N Y_D Y_{12}/M_N$ for $M_N \gg M_{\text{EW}}$. The maximal δa_μ therefore decreases as $1/M_D$ for large doublet masses, but is constant in the limit of large singlet masses. In general, it is thus impossible to rule out mixing vector fermions as an explanation for the discrepancy Δa_μ with any indirect observable that decouples in the high-mass regime. Direct searches for vector fermions at the LHC are not able to probe the mass regime far above $M_{1,2} \sim 500 - 600$ GeV (see Section 6). Therefore an explanation of Δa_μ with mixing vector fermions and new sources of flavor violation cannot be excluded even the 14-TeV LHC.

5 Two new fields with different spin

Besides the case with two mixing fermions discussed in the previous section, two new fields with different spins can yield significant contributions to a_μ . In this section, we discuss combinations of one vector fermion and one new scalar or vector boson. These two-field contributions to a_μ are dominant in scenarios where effects of a single new field are constrained by other observables or suppressed by symmetries. The corresponding Feynman diagrams are shown in Figure 4; analytic expressions are given in Table 4 in Appendix A.

Constraints on the coupling of one SM lepton to a new vector fermion and a vector or scalar boson, $\bar{\ell}\psi V/\phi$, can be derived from $e^+e^- \rightarrow \ell^+\ell^-$ processes measured at LEP [15].⁹ In the limit $M_{V,\phi,\psi} \gg \sqrt{s}$, new-physics effects in these processes can be described by effective four-lepton interactions

$$\mathcal{H}_{\text{eff}} = \sum_{A,B=L,R} \mathcal{C}_{AB} \mathcal{O}_{AB}, \quad \mathcal{O}_{AB} = (\bar{e}\gamma_\mu e_A)(\bar{\ell}\gamma^\mu \ell_B), \quad (32)$$

⁹We restrict ourselves to leptons $\ell = \mu, \tau$ in the final state, which lead to stronger constraints on LL and RR interactions than $\ell = e$.

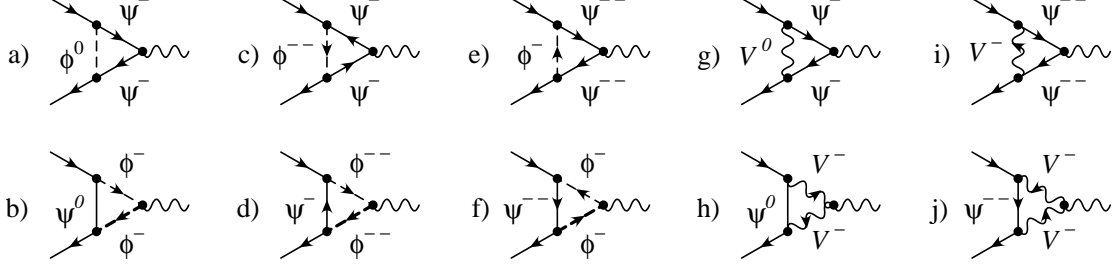


Figure 4: Contributions to a_μ from two new particles with different spins in the vertex loop.

where \mathcal{O}_{AB} are local operators and $A, B = L, R$ indicate the chirality of the lepton fields. Two-particle couplings $\bar{\ell}\psi V/\phi$ generate four-lepton contact terms at the one-loop level through the box diagrams in Figure 5, with the corresponding Wilson coefficients $\mathcal{C}_{AB} \sim g^4/(16\pi^2 M_{V,\phi}^2)$. Due to the loop suppression, two-particle couplings are expected to be less constrained than the one-particle couplings discussed in Section 3, which induce four-lepton interactions at the tree level, yielding $\mathcal{C}_{AB} \sim g^2/M_{V,\phi}^2$. As we will see, constraints from four-lepton interactions can still have a considerable impact on two-particle effects on a_μ , in particular in scenarios where the coupling g is sizeable. The four-lepton interaction terms for the two-particle combinations relevant in this section are listed in Table 7 in Appendix B. Let us discuss the different scenarios one by one.

Neutral scalar (ϕ^0) and charged fermion (ψ^\pm): This scenario can contribute to a_μ through the diagram in Figure 4 (a) with the corresponding couplings,

$$\mathcal{L} \supset -Y \bar{\ell}_L \phi^0 \psi_R^- + \text{h.c.} \quad \text{or} \quad \mathcal{L} \supset -Y \bar{\ell}_R \phi^0 \psi_L^- + \text{h.c.} \quad (33)$$

The former coupling applies if either of the new particles is part of an $SU(2)$ doublet and the other one is a singlet, whereas the latter coupling is relevant if both new particles are either singlets or part of a doublet. The chirality of the SM lepton is thus determined by the electroweak properties of the new particles. The discrepancy Δa_μ in (1) can be explained at the one-(two-)sigma level for

$$Y > 1.9 \text{ (1.5)}, \quad M_{\phi,\psi} > 100 \text{ GeV}. \quad (34)$$

In Figure 6 (a), we display the parameter space for $\phi^0 + \psi^\pm$ that accommodates Δa_μ at the one- and two- and sigma level (green and yellow areas) for $Y \leq \sqrt{4\pi}$ in terms of the scalar and fermion masses M_ϕ and M_ψ . Constraints from four-lepton contact interactions are absent in this scenario due to a cancellation between the two contributing box diagrams for vanishing external momenta.

Charged scalar (ϕ^\pm) and neutral fermion (ψ^0): This combination of fields contributes to a_μ through the diagram in Figure 4 (b) with the following couplings,

$$\mathcal{L} \supset -Y \bar{\ell}_L \phi^- \psi_R^0 + \text{h.c.} \quad \text{or} \quad \mathcal{L} \supset -Y \bar{\ell}_R \phi^- \psi_L^0 + \text{h.c.} \quad (35)$$

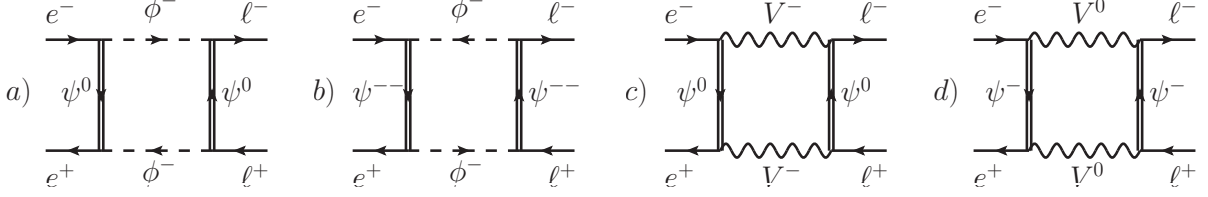


Figure 5: One-loop contributions to effective four-lepton interactions $eell$.

The electroweak properties determine the structure of the coupling as in the previous case with $\phi^0 + \psi^\pm$. The contribution to a_μ is negative and cannot explain the observed discrepancy.

Scalar doublet (ϕ_D) and fermion doublet (ψ_D): The two doublets defined in (14) and (22) couple to right-handed SM leptons via

$$\mathcal{L} \supset -Y \overline{\psi_{D,L}} \phi_D \ell_R + \text{h.c.} \quad (36)$$

The sum of contributions from the neutral and charged components of the scalar doublet, Figure 4 (a,b), yields a positive correction to a_μ . However, the result is too small to explain the discrepancy in (1). Furthermore, constraints on $eell$ interactions at LEP exclude an explanation of Δa_μ within two sigma. Any significant contribution to a_μ from $\phi_D + \psi_D$ is thereby strongly disfavored.

Scalar doublet (ϕ_D) and fermion adjoint triplet (ψ_A): Contributions of $\phi_D + \psi_A$ to a_μ , with ψ_A defined in (23), correspond to the diagrams in Figure 4 (a,b) with the coupling

$$\mathcal{L} \supset -Y \tilde{\phi}_D^\dagger \overline{\psi_{A,R}} L_L + \text{h.c.} \quad (37)$$

Due to the different SU(2) structure, the (negative) contribution of $\phi_D^- + \psi_A^0$ is reduced by a factor of $(\sqrt{2})^{-4}$ with respect to the previous scenario $\phi_D + \psi_D$. A priori, the discrepancy Δa_μ can be explained at the one-(two)-sigma level for

$$Y > 2.7 (2.1), \quad M_{\phi,\psi} > 100 \text{ GeV}. \quad (38)$$

Figure 6 (b) shows the full parameter space that covers Δa_μ . Four-lepton contact interactions are generated by the contribution of $\phi_D^- + \psi_A^0$ in Figure 5 (a). LEP bounds on $eell$ interactions (shaded gray) exclude all of the available parameter space that explains Δa_μ at the two-sigma level. In the low-mass range $M_{\phi,\psi} \sim \sqrt{s} \sim 200 \text{ GeV}$, constraints from $eell$ interactions should be taken with care, since the dynamics of the new particles beyond the zero-momentum approximation are important. For our purposes, which focus on LHC constraints, it suffices to state that effects from $\phi_D + \psi_A$ on a_μ are strongly suppressed, if not ruled out by LEP bounds on $eell$ interactions.

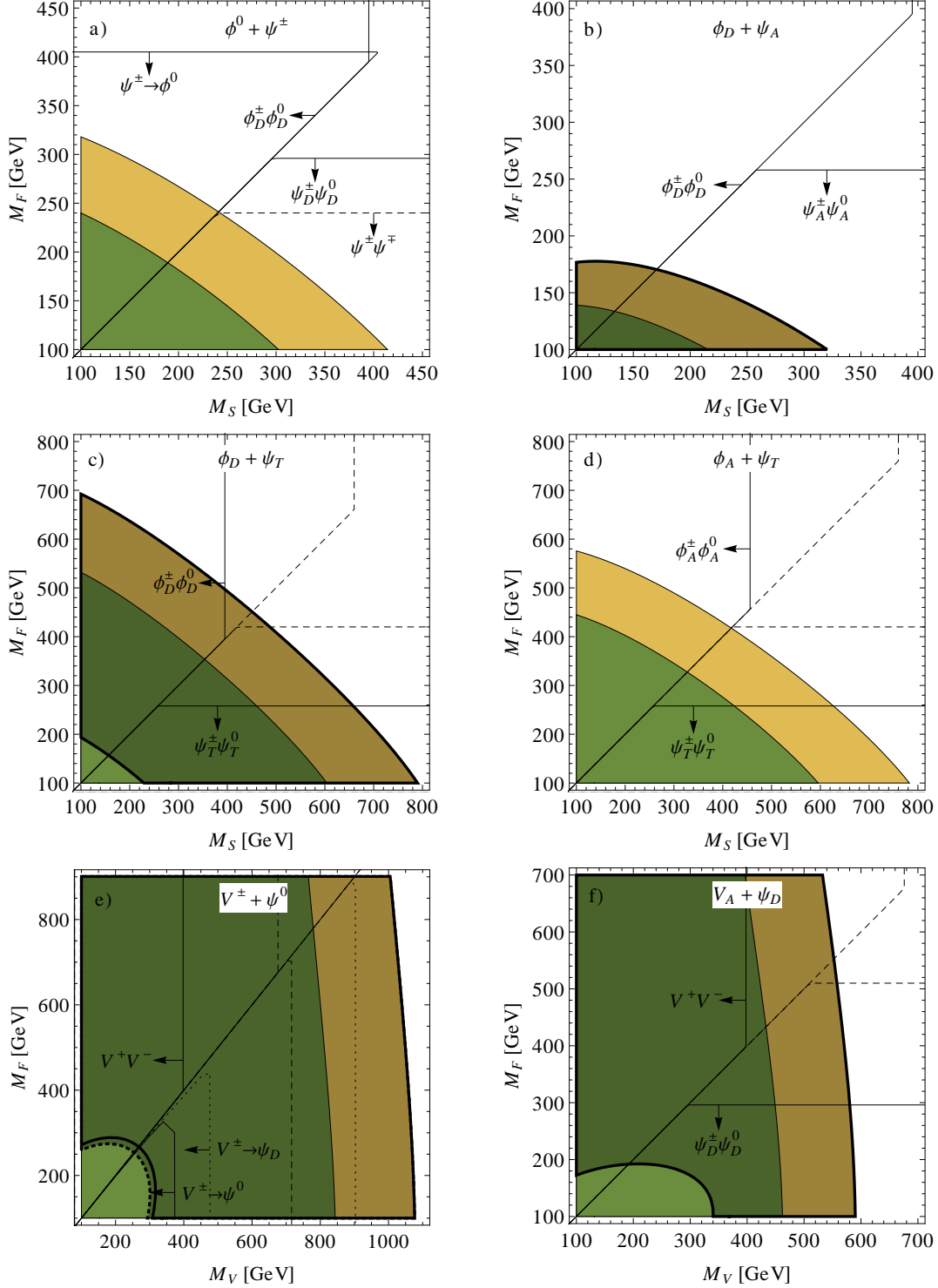


Figure 6: Contributions to a_μ from two new fields with different spin for $Y, g \leq \sqrt{4\pi}$ (green: 1σ, yellow: 2σ region). The gray area with bold boundaries is disfavored by LEP constraints on $ee\ell\ell$ contact interactions to explain Δa_μ within the 1σ range. Lower mass bounds at 95% C.L. from direct searches at the 8-TeV LHC and projections for 14 TeV (see Section 6) are displayed as plain and dashed black lines (dotted for $V^\pm + \psi_D$), respectively.

Scalar doublet (ϕ_D) and fermion triplet (ψ_T): Compared to the previous scenarios, the presence of the triplet ψ_T with hypercharge -1 , defined in (24), introduces new contributions to a_μ with doubly-charged leptons through the coupling

$$\mathcal{L} \supset -Y \phi_D^\dagger \overline{\psi_{T,R}} L_L + \text{h.c.} \quad (39)$$

The corresponding diagrams are given in Figure 4 (a,e,f). The scenario $\phi_D + \psi_T$ can explain Δa_μ at the one-(two-)sigma level for

$$Y > 1.0 (0.8), \quad M_{\phi,\psi} > 100 \text{ GeV}. \quad (40)$$

The full parameter space is given in Figure 6 (c). Constraints from $e\ell\ell$ interactions are due to box diagrams with $\phi_D^- + \psi_T^{--}$, as displayed in Figure 5 (b).¹⁰ They exclude large parts (the gray area) of the parameter space for Δa_μ . Potential contributions at the one-sigma level are thereby confined to a small region of the parameter space with light masses $M_{\phi,\psi} \sim 100 - 150 \text{ GeV}$.

Scalar adjoint triplet (ϕ_A) and fermion doublet (ψ_D): The scenario with a scalar triplet ϕ_A with hypercharge 0 and a fermion doublet ψ_D contributes to a_μ through the diagrams in Figure 4 (a,b) with the coupling

$$\mathcal{L} \supset -Y \overline{\psi_{D,R}} \phi_A L_L + \text{h.c.}, \quad \phi_A = \begin{pmatrix} \phi_A^0/\sqrt{2} & \phi_A^+ \\ \phi_A^- & -\phi_A^0/\sqrt{2} \end{pmatrix}. \quad (41)$$

The result is negative and cannot accommodate Δa_μ .

Scalar adjoint triplet (ϕ_A) and fermion triplet (ψ_T): Contributions to a_μ arise from the diagrams in Figure 4 (a,b,e,f) through the coupling

$$\mathcal{L} \supset -Y \text{tr}\{\phi_A^\dagger \overline{\psi_{T,L}}\} \ell_R. \quad (42)$$

This scenario can accommodate Δa_μ in the one-(two-)sigma region with couplings

$$Y > 1.1 (0.9), \quad M_{\phi,\psi} > 100 \text{ GeV}. \quad (43)$$

The complete parameter range with perturbative couplings is shown in Figure 6 (d). Constraints from four-lepton interactions are absent due to cancellations among box diagrams with $\phi_A^0 + \psi_T^-$ and among diagrams with ϕ_A^- and leptons ψ_T^0, ψ_T^{--} .

Scalar triplet (ϕ_T) and fermion doublet (ψ_D): The diagrams for a_μ with ϕ_T defined in (19) and ψ_D are given in Figure 4, induced by the coupling

$$\mathcal{L} \supset -Y \overline{\psi_{D,L}} \phi_T i\sigma_2 L_L^c + \text{h.c.} \quad (44)$$

The contribution to a_μ is negative and thus not appropriate to explain Δa_μ .

¹⁰Contributions from ϕ_D^0 and ψ_T^- cancel between a box diagram similar to the one in Figure 5 (a) with $\phi^- \rightarrow \phi_D^0$ and $\psi^0 \rightarrow \psi_T^-$ and the diagram with crossed ϕ_D^0 lines, as in the scenario $\phi^0 + \psi^\pm$ described above.

Scalar triplet (ϕ_T) and fermion adjoint triplet (ψ_A): These two triplets induce corrections to a_μ through the diagrams in Figure 4 (a,b,c,d) with the coupling

$$\mathcal{L} \supset -Y \text{tr}\{\phi_T^\dagger \overline{\psi_{A,L}}\} \ell_R. \quad (45)$$

Also in this case, the contribution to a_μ is negative and not able to account for the observed discrepancy.

Neutral vector singlet (V^0) and charged fermion (ψ^\pm): This combination contributes to a_μ through the diagram in Figure 4 (g). The fermion ψ^\pm can be either a weak singlet or part of a doublet, which determines the coupling

$$\mathcal{L} \supset -g_R \overline{\psi_R^-} \gamma^\mu \ell_R^- V_\mu^0 + \text{h.c.} \quad \text{or} \quad \mathcal{L} \supset -g_L \overline{\psi_{D,L}} \gamma^\mu L_L V_\mu^0 + \text{h.c.}, \quad (46)$$

respectively. The resulting contribution to a_μ is negative, ruling out $V^0 + \psi^\pm$ as an explanation of Δa_μ .

Charged vector singlet (V^\pm) and neutral fermion (ψ^0): The Feynman diagram for a_μ in this scenario is given in Figure 4 (h). Similarly to the previous case, the vector fermion ψ^0 can be a weak singlet or part of a doublet, yielding the chiral couplings

$$\mathcal{L} \supset -g_R \overline{\psi_R^0} \gamma^\mu \ell_R^+ V_\mu^+ + \text{h.c.} \quad \text{or} \quad \mathcal{L} \supset -g_L \overline{\psi_{D,L}} \gamma^\mu i\sigma_2 L_L^c V_\mu^- + \text{h.c.}, \quad (47)$$

respectively. The scenario $V^\pm + \psi^0$ can accommodate Δa_μ in the one-(two)-sigma region with couplings

$$g_{R,L} > 0.5 \text{ (0.4)}, \quad M_{V,\psi} > 100 \text{ GeV}, \quad (48)$$

as displayed for the full parameter space in Figure 6 (e). Notice that the dependence of a_μ on the fermion mass M_ψ is very weak. Constraints from $eell$ contact interactions mediated by the box diagram in Figure 5 (c) exclude large parts of the parameter space (the gray area in Figure 6 (e), whose plain contour corresponds to the (right-chiral) fermion singlet case; the dotted contour depicts the (left-chiral) doublet case). Since the couplings to accommodate Δa_μ with light new particles are relatively weak, $eell$ constraints leave open a mass range of $M_{V,\psi} \sim 100 - 300$ GeV to explain Δa_μ within its one-sigma limits.

Vector adjoint triplet (V_A) and fermion doublet (ψ_D): This scenario combines the contributions of the previous two cases from Figure 4 (g,h). The corresponding coupling to SM leptons is left-chiral,

$$\mathcal{L} \supset -g_L \overline{\psi_{D,L}} \gamma_\mu V_A^\mu L_L + \text{h.c.}, \quad V_A = \begin{pmatrix} V_A^0/\sqrt{2} & V_A^+ \\ V_A^- & -V_A^0/\sqrt{2} \end{pmatrix}. \quad (49)$$

This scenario can explain Δa_μ in the one-(two)-sigma region, provided

$$g_L > 0.9 \text{ (0.7)}, \quad M_{V,\psi} > 100 \text{ GeV}. \quad (50)$$

Compared to the scenario $V^\pm + \psi^0$, the parameter space is shifted towards lower masses, see Figure 6 (e). Four-lepton contact interactions induced by the diagrams in Figure 5 (c,d) restrict the one-sigma region for Δa_μ to the mass range $M_V \sim 100 - 300$ GeV, $M_\psi \sim 100 - 200$ GeV.

Vector adjoint triplet (V_A) and fermion triplet (ψ_T): The two triplets defined in (24) and (49) couple to muons through

$$\mathcal{L} \supset -g_R \overline{\psi_{T,R}} \gamma_\mu V_A^\mu \ell_R^- + \text{h.c.} \quad (51)$$

and contribute to a_μ via the diagrams in Figure 4 (g,h,i,j). The result is negative and cannot accommodate the discrepancy Δa_μ .

6 LHC constraints

In the previous sections, the minimal new-physics scenarios that could potentially accommodate the muon magnetic moment anomaly in (1) have been identified. These are

- for one new field: V^\pm ;
- for two mixed fermion fields: none;
- for two different-spin fields: $\phi^0 + \psi^\pm$, $\phi_D + \psi_A$, $\phi_D + \psi_T$, $\phi_A + \psi_T$, $V^\pm + \psi^0$ and $V_A + \psi_D$.

This section is devoted to investigating how the preferred parameter space for explaining Δa_μ in these scenarios is constrained by current LHC data and may be further probed with the future 14-TeV run. As mentioned in Section 5, in some two-field cases the allowed parameter space is already severely limited by bounds on loop-induced four-lepton interactions from LEP2 (the gray regions in Figure 6). However, these four-lepton corrections may conceivably be canceled by tree-level contributions from the exchange of a very heavy neutral vector boson V^0 (which would have a minimal effect on a_μ , see Section 3). Therefore we will also explore the parameter space that is nominally excluded by four-lepton interactions.

To minimize the model dependence, we focus on production of the new particles through the Drell-Yan process, which involves only gauge couplings. In particular, charged particles X^\pm can be pair-produced through the partonic process $q\bar{q} \rightarrow X^+X^-$ via s-channel photon and Z -boson exchange. In the case of SU(2) multiplets with both charged and neutral components, one also has the associated production $q\bar{q}' \rightarrow X^\pm X^0$ via s-channel W^\pm exchange.

In scenarios with two new fields, we will always look for constraints on the pair production of the lighter of the two. In this way, we circumvent cascade decays from the heavier to the lighter field, which would lead to more complex signatures. The scenarios $\phi^0 + \psi^\pm$ and $V^\pm + \psi^0$ involve a new particle that is a SM gauge singlet. In this special case, Drell-Yan production of singlet pairs is not possible, so that we will instead consider cascade decays from the heavier charged particle. Due to the fact that relatively large couplings in the new-physics sector are required to explain Δa_μ , the decay into the singlet is expected to be the dominant decay mode of the heavy charged particle.

Since the new fields need to couple to muons, we generically expect them to decay leptonically. In addition, the possible decay modes are constrained by MFV. For a neutral scalar, ϕ^0 , these two considerations naturally imply the decay $\phi^0 \rightarrow \ell^+\ell^-$, $\ell = e, \mu, \tau$, which is universal in lepton flavor. Similarly, the characteristic decay of a charged scalar, ϕ^\pm , is given

by $\phi^+ \rightarrow \ell^+ \nu_\ell$, $\ell = e, \mu, \tau$. The typical decays of new heavy vector bosons are completely analogous, i.e. $V^0 \rightarrow \ell^+ \ell^-$ and $V^+ \rightarrow \ell^+ \nu_\ell$. For heavy fermions, MFV mandates that they transform in the fundamental representation of the lepton flavor symmetry, so that there are three flavor copies ψ_ℓ , $\ell = e, \mu, \tau$. The characteristic decay modes for neutral and charged fermions are given by $\psi^0 \rightarrow \nu Z, \nu H, \ell^- W^+$ and $\psi^- \rightarrow \ell^- Z, \ell^- H, \nu W^-$, respectively, with the branching fractions determined by the SU(2) representation of $\psi^{0,\pm}$ (see below). Lacking public results on LHC searches for doubly-charged fermions, we will instead constrain scenarios with triplet fermions through their neutral and singly-charged components.

Table 2 summarizes the production and decay modes considered for deriving the LHC constraints in this section. For concreteness, we will assume that there are no additional decay modes besides those listed in the table. For the new heavy scalar and vector bosons, MFV would in principle also permit decay channels into quarks, SM weak gauge bosons, or Higgs bosons. Furthermore, there may be exotic decays into additional light states of the new-physics sector that do not play any role for a_μ . Therefore the reader should bear in mind that the presence of any decay channels beyond those listed in Table 2 would reduce the observable signal at the LHC and thus weaken the limits presented below.

6.1 Constraints from existing 8-TeV LHC data

To derive the constraints on the viable parameter space of our simplified scenarios from existing LHC data, we use results published by the ATLAS and CMS collaborations for new-physics searches in particular models, and recast them to the processes considered here. The resulting bounds on the masses of new particles are illustrated in Figures 3 and 6.

- $pp \rightarrow \phi^\pm \phi^0 \rightarrow \ell^\pm \nu_\ell \ell'^+ \ell'^-$: This process can be constrained using results of a search for supersymmetric charginos and neutralinos by ATLAS based on a signature with three leptons and missing energy [22] (for a similar analysis by CMS, see [23]). The strongest limits are obtained in the signal region referred to as SRnoZc in [22]. We have used CALCHEP to compute the signal rate in our scenario, implementing these cuts together with basic selection cuts from [22]. We assume that the scalars decay into the three generations of SM leptons with equal probability and there are no other decay channels. The mass bound was determined by finding the mass which generated the 95% C.L. upper limit on the signal cross section as given in Table 4 of [22].

We find that the current ATLAS data sets a bound on the mass of a scalar doublet, $M_{\phi_D} > 395$ GeV at 95% C.L. This eliminates all allowed parameter space of Δa_μ for $\phi_D + \psi^\pm$ and $\phi_D + \psi_A$ (both for $M_\phi < M_\psi$), and part of the allowed parameter space for $\phi_D + \psi_T$ ($M_\phi < M_\psi$). The bound for a scalar weak triplet is $M_{\phi_A} > 456$ GeV at 95% C.L. Due to the isospin-enhanced coupling to gauge bosons, the constraint is stronger than for the doublet. It excludes the entire parameter space of Δa_μ in the scenario $\phi_A + \psi_T$ for $M_\phi < M_\psi$.

- $pp \rightarrow \psi^\pm \psi^0 \rightarrow Z \ell^\pm W^\pm \ell^\mp \rightarrow \ell'^+ \ell'^- \ell^\pm W^\pm \ell^\mp$: This process is very similar to pair production of heavy fermions in the type-III seesaw model. Limits on this model have been obtained by ATLAS [24] and CMS [25]. Here the ATLAS analysis has been used to put

Scenario	Production	LHC8	LHC14
V^\pm	$pp \rightarrow V^+V^-$	$M_V > 398 \text{ GeV}$	$M_V > 676 \text{ GeV}$
$\phi^0 + \psi^\pm$	$M_\psi < M_\phi: pp \rightarrow \psi^+\psi^-$	—	×
	$M_\psi > M_\phi: pp \rightarrow \psi^+\psi^- \rightarrow \ell^+\phi^0 \ell^-\phi^0$	×	×
$\phi^0 + \psi_D$	$M_\psi < M_\phi: pp \rightarrow \psi^\pm\psi^0$	×	×
	$M_\psi > M_\phi: pp \rightarrow \psi^+\psi^- \rightarrow \ell^+\phi^0 \ell^-\phi^0$	×	×
$\phi_D + \psi^\pm$	$M_\psi < M_\phi: pp \rightarrow \psi^+\psi^-$	—	×
	$M_\psi > M_\phi: pp \rightarrow \phi^\pm\phi^0$	×	×
$\phi_D + \psi_A$	$M_\psi < M_\phi: pp \rightarrow \psi^\pm\psi^0$	×	×
	$M_\psi > M_\phi: pp \rightarrow \phi^\pm\phi^0$	×	×
$\phi_D + \psi_T$	$M_\psi < M_\phi: pp \rightarrow \psi^\pm\psi^0$	$M_\psi > 258 \text{ GeV}$	$M_\psi > 420 \text{ GeV}$
	$M_\psi > M_\phi: pp \rightarrow \phi^\pm\phi^0$	$M_\phi > 380 \text{ GeV}$	×
$\phi_A + \psi_T$	$M_\psi < M_\phi: pp \rightarrow \psi^\pm\psi^0$	$M_\psi > 258 \text{ GeV}$	×
	$M_\psi > M_\phi: pp \rightarrow \phi^\pm\phi^0$	×	×
$V^\pm + \psi^0$	$M_V < M_\psi: pp \rightarrow V^+V^-$	$M_V > 398 \text{ GeV}$	$M_V > 676 \text{ GeV}$
	$M_V > M_\psi: pp \rightarrow V^+V^- \rightarrow \ell^+\psi^0 \ell^-\psi^0$	$M_V > 373 \text{ GeV}$	$M_V > 716 \text{ GeV}$
$V^\pm + \psi_D$	$M_V < M_\psi: pp \rightarrow V^+V^-$	$M_V > 398 \text{ GeV}$	$M_V > 676 \text{ GeV}$
	$M_V > M_\psi: pp \rightarrow V^+V^- \rightarrow \ell^+\psi^0 \ell^-\psi^0$	$M_V > 476 \text{ GeV}$	$M_V > 903 \text{ GeV}$
$V_A + \psi_D$	$M_V < M_\psi: pp \rightarrow V^+V^-$	$M_V > 398 \text{ GeV}$	×
	$M_V > M_\psi: pp \rightarrow \psi^\pm\psi^0$	$M_\psi > 296 \text{ GeV}$	×

Decay	$\phi^0 \rightarrow \ell^+\ell^-$	$V^0 \rightarrow \ell^+\ell^-$	$\psi^0 \rightarrow \nu Z, \nu H, \ell^\pm W^\mp$
	$\phi^\pm \rightarrow \ell^\pm \nu$	$V^\pm \rightarrow \ell^\pm \nu$	$\psi^\pm \rightarrow \ell^\pm Z, \ell^\pm H, \nu W^\pm$

Table 2: LHC production (top) and typical decay process (bottom) for the new particles in the one- and two-field scenarios that can explain the muon magnetic moment anomaly. Cases that are excluded at two sigma by 8-TeV LHC data or can be probed conclusively at 14 TeV are marked by a cross. Wherever the two-sigma range of Δa_μ is not fully covered, we display the lower mass bounds as obtained from the analyses described in the text.

limits on the production of weak doublet and triplet vector fermions. The cross sections for $pp \rightarrow \psi^\pm \psi^0$ were computed in CALCHEP, assuming that the vector fermions are lepton flavor triplets, as mandated by MFV. Since the experimental searches are sensitive to both electrons and muons, this leads to a factor of two for the production rate. The computed numbers for cross section times branching ratio were compared to the observed 95% C.L. line in Figure 3 of [24].

For triplet fermions, the branching ratios are given by $\mathcal{B}(\psi^\pm \rightarrow Z\ell^\pm) = 1/4$ and $\mathcal{B}(\psi^0 \rightarrow W^\pm \ell^\mp) = 1/2$, which leads to the limit $M_{\psi_{A,T}} > 258$ GeV. Doublet fermions have a smaller production cross section, but larger branching ratios $\mathcal{B}(\psi^\pm \rightarrow Z\ell^\pm) = 1/2$ and $\mathcal{B}(\psi^0 \rightarrow W^\pm \ell^\mp) = 1$, resulting in the limit $M_{\psi_D} > 296$ GeV. For the cases with a new fermion and a new scalar field, these bounds eliminate all allowed parameter space for $\phi_D + \psi_A$ and part of the parameter space for $\phi_D + \psi_T$ and $\phi_A + \psi_T$ (all for $M_\psi < M_\phi$). Similarly, they exclude part of the viable parameter region for $V_A + \psi_D$ (for $M_\psi < M_V$).

- $pp \rightarrow \psi^\pm \psi^\mp \rightarrow Z\ell^\pm Z/H\ell^\mp \rightarrow \ell'^+ \ell'^- \ell^\pm \ell^\mp + \text{hadrons}$: For charged singlet fermions, the process described in the previous item does not exist. However, if one fermion in $\psi^+ \psi^-$ decays into a Z boson, while the other one decays into a Z or Higgs boson, one obtains a very similar final-state signature with four leptons, two of which reconstruct the Z invariant mass. Therefore, the cross-section bounds from [24] can be applied approximately also to this case. We assume that the second Z boson decays non-leptonically to account for the second Z veto in the ATLAS analysis. Computing signal cross sections with CALCHEP as above and folding in the branching fractions $\mathcal{B}(\psi^\pm \rightarrow Z\ell^\pm) = \mathcal{B}(\psi^\pm \rightarrow H\ell^\pm) = 1/4$, we find that no limit can be placed on singlet fermion pair production with the result of [24]. This mainly follows from the fact that the production cross section for $\psi^+ \psi^-$, which have only hypercharge but no weak isospin, is suppressed due to the relatively small hypercharges of the initial-state quarks.

- $pp \rightarrow V^+ V^- \rightarrow \ell^+ \ell'^- \nu_\ell \bar{\nu}_{\ell'}$: This process can be constrained from searches for slepton pair production, where each slepton decays into a charged lepton and a neutralino [23, 26]. To translate the slepton limits to vector boson pair production, the cross sections for $pp \rightarrow V^+ V^-$ were computed with CALCHEP, assuming a branching fraction of $1/3$ each into $\ell = e$ and $\ell = \mu$ (the remaining third for $\ell = \tau$ is not used in the experimental analyses). The results were compared to the 95% C.L. upper bounds in Figure 20 (right) in [23] in the case where the neutralino mass is set to zero. With this procedure, the lower limit on the vector boson mass, $M_V > 398$ GeV, is obtained. This mass bound rules out a portion of the allowed parameter space for V^\pm , $V^\pm + \psi^0$ and $V_A + \psi_D$ (for $M_V < M_\psi$).

- $pp \rightarrow V^+ V^- \rightarrow \ell^+ \psi^0 \ell^- \psi^0$ for $V^\pm + \psi^0$: With further decays $\psi^0 \rightarrow W^\pm \ell^\mp$, this process leads to a four-lepton signal. Thus, the masses of V and ψ^0 can be constrained from an ATLAS search [24], which considers events with four or more charged leptons (e, μ) in the final state. Using CALCHEP we computed the signal rate including basic selection cuts as described in [24]. This signal rate was added to the SM background and limits were

determined through comparison with the observed event yield (background and observations are given in the top row of Table 2 in [24]).

If ψ^0 is part of a weak doublet, the branching ratio is $\mathcal{B}(\psi^0 \rightarrow W^\pm \ell^\mp) = 1$. We obtain the limit $M_V > 476$ GeV, provided M_ψ is sufficiently smaller than M_V . For $M_\psi \lesssim M_V$, the decay produces soft leptons, which do not pass the detector cuts. As a result, there is a small gap in the excluded parameter space (see Figure 6 (e)) near the line of $M_V = M_\psi$. The width of the mass gap is 19 GeV for $M_V = 451$ GeV and shrinks to less than 4 GeV for $M_V < 300$ GeV. If ψ^0 is a weak singlet, the branching ratio is reduced to $\mathcal{B}(\psi^0 \rightarrow W^\pm \ell^\mp) = 1/2$. We obtain the less stringent limit $M_V > 373$ GeV, again assuming that M_ψ is sufficiently smaller than M_V . The mass gap is 14 GeV for $M_V = 340$ GeV and shrinks to less than 2 GeV for $M_V < 200$ GeV. This excludes part of the allowed parameter space for the scenarios $V^\pm + \psi_D$ and $V^\pm + \psi^0$ (for $M_V > M_\psi$).

- $pp \rightarrow \psi^+ \psi^- \rightarrow \ell^+ \phi^0 \ell^- \phi^0$ for $\phi^0 + \psi^\pm$: This cascade with the subsequent decay $\phi^0 \rightarrow \ell^+ \ell^-$ is relevant if both the fermion and the (lighter) scalar are weak singlets. We recast the analysis of $pp \rightarrow V^+ V^- \rightarrow \ell^+ \psi^0 \ell^- \psi^0$ described above for $\phi^0 + \psi^\pm$ by adapting the production cross section to a pair of charged fermions. The kinematics of the first decay steps are similar in both scenarios, while the decay of the scalar ϕ^0 typically yields more leptons in the final state compared to the fermion ψ^0 . Therefore we obtain conservative limits if we assume that the event yield passing the detector cuts is similar in both scenarios. The resulting bound on the fermion mass is $M_\psi > 405$ GeV at 95% C.L. This excludes the entire parameter region for Δa_μ in the two-singlet scenario $\phi^0 + \psi^\pm$ with $M_\psi > M_\phi + 5$ GeV. Since the cross section for a pair of charged doublet fermions is about a factor of two larger than for singlet fermions, the same analysis also excludes the scenario $\phi^0 + \psi_D$ ($M_{\psi_D} > M_\phi$) as a possible explanation of Δa_μ .

The mass bounds obtained for each scenario with 8-TeV data are listed in Table 2. Excluded (unconstrained) scenarios are marked by a cross (a hyphen). As is apparent from the table, the scenarios $\phi_D + \psi_D$ and $\phi_D + \psi_A$ are already excluded at the two-sigma level by LHC searches. Taking LEP constraints from one-loop $e\ell\ell$ contact terms into account, all scenarios are excluded but those with a neutral or weak adjoint scalar, where contributions to $e\ell\ell$ interactions cancel. In some scenarios, especially those with new vector bosons, the viable parameter space reaches out to mass scales in the TeV range. As we will show in the following section, the higher collision energy at the 14-TeV LHC will be beneficial to test those high-mass regions.

6.2 Projections for the 14-TeV LHC

For the 14-TeV projections, we follow the strategy of [27]. Starting from the existing 8-TeV searches by ATLAS and CMS (referenced in the previous subsection), the expected event yields were obtained by scaling the luminosity to 300 fb^{-1} and multiplying with the ratio of cross sections $\sigma_{\text{sig(bkg)}}(14 \text{ TeV})/\sigma_{\text{sig(bkg)}}(8 \text{ TeV})$. The total production cross section $\sigma_{\text{sig(bkg)}}(\sqrt{s})$ for the signal (dominant backgrounds) at the pp CM energy of \sqrt{s} was com-

puted with CALCHEP. This approach assumes that the selection efficiency for the signal and background will remain similar when going from an 8-TeV to a 14-TeV analysis. While this assumption is admittedly rather ad hoc, a more refined estimation would require a full-fledged simulation, which is beyond the scope of this paper. Since the signal cross section varies very rapidly as a function of the produced particles' masses, we believe that our projected mass limits will not be strongly influenced by the uncertainties in the selection efficiency and thus should give a meaningful indication of the reach of the 14-TeV LHC. Furthermore, several of the existing ATLAS and CMS analyses used above are not optimized for our new-physics signatures, so that we expect our projected bounds to be rather conservative.

Using this procedure to re-scale the analyses of the previous subsection, we obtain the following expected exclusion limits for the 14-TeV LHC:

- $pp \rightarrow \phi^\pm \phi^0 \rightarrow \ell^\pm \nu_\ell \ell'^+ \ell'^-$: For scalar doublets, we obtain the projected mass bound of $M_{\phi_D} > 660$ GeV. If no signal is observed, this will rule out the entire parameter space for Δa_μ in the scenario $\phi_D + \psi_T$ for $M_\phi < M_\psi$. The projection for the scalar adjoint triplet pushes the mass limit up to $M_{\phi_A} > 760$ GeV.
- $pp \rightarrow \psi^\pm \psi^0 \rightarrow Z \ell^\pm W^\pm \ell^\mp \rightarrow \ell'^+ \ell'^- \ell^\pm W^\pm \ell^\mp$: For triplet fermions, the projected mass bound is $M_{\psi_{A,T}} > 420$ GeV, while for doublet fermions we obtain $M_{\psi_D} > 510$ GeV. These estimates probe the entire parameter region for $\phi_A + \psi_T$ and almost the complete region for $\phi_D + \psi_T$ and $V_A + \psi_D$ (all for $M_\psi < M_{\phi,V}$).
- $pp \rightarrow \psi^\pm \psi^\mp \rightarrow Z \ell^\pm Z / H \ell^\mp \rightarrow \ell'^+ \ell'^- \ell^\pm \ell^\mp + \text{hadrons}$: The increased luminosity and production energy at the 14-TeV LHC allow us to set a first lower bound on the mass of electroweak singlet fermions, $M_\psi > 240$ GeV. It covers the full parameter space of Δa_μ for $\phi^0 + \psi^\pm$ and $\phi_D + \psi^\pm$ (both for $M_\psi < M_\phi$).
- $pp \rightarrow V^+ V^- \rightarrow \ell^+ \ell'^- \nu_\ell \bar{\nu}_\ell$: The projected bound for the production of two new vector fermions is $M_V > 676$ GeV. This will probe the full parameter space of Δa_μ in the scenario $V_A + \psi_D$ for $M_V < M_\psi$ and a significant portion of parameter space in the scenarios V^\pm and $V^\pm + \psi^0$ (for $M_V < M_\psi$).
- $pp \rightarrow V^+ V^- \rightarrow \ell^+ \psi^0 \ell^- \psi^0$: The projected mass limits reach $M_V > 716$ GeV for a singlet fermion and $M_V > 903$ GeV for a doublet fermion (both for $M_V > M_\psi$). This corresponds to part of the parameter space for the scenarios $V^\pm + \psi^0$ and $V^\pm + \psi_D$.

The limits on the parameter space of each specific scenario are marked in Figures 3 and 6 as dashed lines. From the plots and from our summary in Table 2, it is apparent that the 14-TeV LHC has a strong potential to conclusively probe most viable scenarios for Δa_μ . All scenarios with new scalars and a vector boson triplet can be tested (the small open corner of parameter space for $\phi_D + \phi_T$ will presumably be closed with refined analyses). In

scenarios with a singlet vector boson, the 14-TeV data can push the mass bounds to regions of parameter space where strong couplings $g_R \gtrsim 3.0$ or $g_L \gtrsim 3.8$ to leptons are required to explain Δa_μ at two sigma. These regions, however, are already excluded by LEP searches for four-lepton contact interactions, unless those constraints are relaxed by additional fields in a specific model. Combining LEP and 14-TeV LHC data, all of the minimal models considered in this work can thus be either excluded or conclusively tested.

7 $\tan\beta$ -enhanced corrections

In Sections 3–5 we found that a weakly coupled new-physics explanation for the a_μ discrepancy requires that at least some of the new particles have masses of a few 100 GeV, with upper 95% C.L. bounds typically significantly below 1 TeV. As a result, the LHC can search for these particles in a fairly model-independent way, as we discussed in the previous section.

However, in some models the correction to a_μ can be enhanced by a factor $\tan\beta \gg 1$, where $\tan\beta = v_2/v_1$ is the ratio of the vevs of two Higgs doublets. The best-known example of this kind is the Minimal Supersymmetric Standard Model (MSSM) [28, 29]. In order to realize $\tan\beta$ -enhanced contributions to a_μ , the new-physics sector has to fulfill a number of conditions:

- It needs to contain a second Higgs doublet. The muon receives its mass from coupling to the Higgs doublet with the smaller vev, $m_\mu = y_\mu v_1/\sqrt{2}$. The Yukawa coupling $y_\mu = \sqrt{2}m_\mu/(v \cos\beta) \approx \sqrt{2}m_\mu \tan\beta/v$ is thus enhanced by $\tan\beta$, which leads to the corresponding enhancement of the a_μ correction.
- There must be additional terms that break the chiral symmetry of the leptons. In the MSSM this role is played by the μ term in the superpotential.
- The relevant one-loop diagrams should contain one $\tan\beta$ -enhanced coupling proportional to y_μ (in accordance with MFV). The other couplings in the diagram should be of weak strength (i.e. not involving additional small muon Yukawa couplings). Typically this requires mixing between several new particles, such as gaugino–higgsino mixing or L-sfermion–R-sfermion mixing in the MSSM.

For the example of the MSSM, analytic expressions for δa_μ can be found for instance in [29]. Taking values of $\tan\beta$ in the range $30 \lesssim \tan\beta \lesssim 100$, the observed discrepancy Δa_μ in (1) can be accommodated in the MSSM even if the masses of the particles in the loop are of $\mathcal{O}(1 \text{ TeV})$. Owing to these large masses, it becomes more difficult to conclusively test this scenario at the LHC.

On the other hand, the MSSM (or any other model that can produce $\tan\beta$ -enhanced corrections to a_μ) is clearly more complex than the scenarios discussed in the previous sections of this paper, since it requires the introduction of four or more fields beyond the SM (the second Higgs doublet, and a boson and two mixing fermion fields in the loop, or a fermion and two mixing boson fields in the loop). This added complexity leads to a richer phenomenology and potential new signatures at the LHC, which require a dedicated (and

more model-dependent) analysis. We refer the reader to the pertinent literature for the MSSM [30], where these questions have been studied in detail.

8 Conclusions

The goal of this work was to determine to what extent an explanation of the a_μ anomaly in terms of new particles around the electroweak scale can be probed with existing and expected data at the LHC. We have followed a model-independent approach and investigated perturbative scenarios with one or two new fields with spin and weak isospin up to one. Throughout this work, we have assumed that lepton flavor violation in the couplings of those new fields is minimal, in the sense of introducing no new sources of flavor violation besides the lepton Yukawa couplings in the SM. The assumption of MFV protects the process $\mu \rightarrow e\gamma$ from overly large effects, as discussed in Section 2.2. It requires that new vector leptons transform as the fundamental representation of the flavor group, which has consequences on their production and decay rates at the LHC. MFV also affects constraints from e^+e^- collisions at LEP, which are based on flavor-universal couplings of new vector and scalar bosons to leptons.

In a first step, we have identified those models which can explain the discrepancy Δa_μ within its two-sigma range. A number of cases yield negative contributions to a_μ or are too small to explain Δa_μ with perturbative couplings. This is true in particular for all scenarios with one new vector lepton weak singlet or triplet and for a scalar triplet, prominent from neutrino mass models of seesaw-type II.

A-priori viable models with one new field are generally strongly constrained by LEP measurements (discussed in Section 3). Searches for resonances in $e^+e^- \rightarrow \ell^+\ell^-$ interactions exclude neutral vector bosons V^0 , often dubbed Z' bosons in a variety of models, and scalar doublets ϕ_D , present in models with extended Higgs sectors, as possible explanations of Δa_μ . Precision measurements of observables at the Z pole set tight limits on the coupling of SM leptons to new vector leptons. This strongly constrains contributions to a_μ in all models with fermion fields. The only viable one-field solution to Δa_μ after LEP is a charged vector boson V^\pm with right-chiral couplings to leptons.

Two vector leptons mixing through a Yukawa coupling Y_ψ are interesting for a_μ , since they lead to contributions enhanced by Y_ψ/y_μ , which easily circumvent LEP constraints (see Section 4). However, MFV implies a direct correlation between effects on a_μ and the electron's anomalous magnetic moment a_e . Through this connection, the precise measurement and SM prediction of a_e prohibit any significant contribution of mixing vector leptons to a_μ . Beyond MFV, the connection to a_e can be relaxed and Δa_μ can be explained for sizeable mixings Y_ψ . Since LEP constraints weaken as the heavy vector leptons decouple from the SM, effects of mixing vector leptons on a_μ may be large even for masses beyond the TeV scale. Such a scenario can therefore not be ruled out at the 14-TeV LHC.

Models with two new fields with different spins are generally less constrained by indirect observables than the previous cases. Still, the coupling of two new fields to leptons can be significantly limited by LEP data through one-loop effects on four-lepton contact interactions.

In Section 5, we found that these constraints exclude large parts of the viable parameter space for a_μ in most scenarios. As far as we know, model-independent constraints from loop-level effects on four-lepton interactions have not been established before. Our results, summarized in Appendix B, may serve as a new general tool to set bounds on the coupling of one lepton to two new weakly-coupling fields in a specific model. Since one-loop effects in four-lepton interactions may be compensated for by another heavy field contributing at tree level, we consider these LEP bounds optional and less rigorous than the bounds from direct searches.

In order to test the remaining viable scenarios at the LHC, we have re-interpreted existing 8-TeV searches for fields that lead to similar signatures (see Section 6). They are mostly based on pair production of the relevant new particles, which subsequently decay into a final state with multiple leptons. We have evaluated the expected event yield with parton-level simulations, assuming that the decay proceeds mainly through the couplings relevant for a_μ and that no further exotic decay channels play a role. In some scenarios with two new fields, we additionally study cascade decays of the heavier new particle into the lighter one, which probe regions of the parameter space that are inaccessible through direct production. All possible models not excluded by indirect observables are summarized in Table 2, together with the production and decay modes we have used to constrain the parameter space for a_μ .

The resulting mass bounds are also listed in Table 2 and illustrated in Figures 3 and 6. Some scenarios are already entirely excluded by 8-TeV data, while for others the viable parameter range is pushed to high masses. Taking loop-induced LEP bounds at face value, the only remaining scenarios are those with a neutral or weak adjoint scalar, where effects on four-lepton interactions cancel. Confining ourselves to robust direct bounds, a number of models, especially those with new vector bosons, cannot be ruled out with 8-TeV data and require further investigation at the 14-TeV LHC. We have thus extrapolated our results with 8-TeV data to the 14-TeV run by rescaling the production cross section and assuming similar event yields. From Table 2, it is apparent that the LHC has the potential to conclusively probe all scenarios with new scalars as a possible explanation of Δa_μ in its 14-TeV run. Models with new vector bosons will, if no discovery is made, be confined to strong couplings and masses around the TeV scale. In order to cover the remaining parameter space within these models, the current analyses may be refined with tailored cuts and the reconstruction of intermediate particles (for a recent approach to reconstruction in the presence of invisible decay products, see for instance [31]).

Beyond our framework of simple models and MFV, solutions to a_μ exist in models with a more complicated structure, such as the MSSM discussed in Section 7. With our model-independent analysis, we provide a guideline for future tests of possible explanations of the a_μ anomaly at the LHC, and a convenient reference to estimate constraints from a_μ on specific similar models.

9 Acknowledgments

This work was supported in part by the National Science Foundation, grant PHY-1212635. Fermilab is operated by Fermi Research Alliance, LLC, under Contract No. DE-AC02-07CH11359 with the United States Department of Energy.

A New-physics contributions to a_μ

In this appendix, we list the one-loop results for a_μ from contributions of one or two of the new fields defined in Table 1. They can be expressed in terms of the loop functions

$$\begin{aligned}
F_{\text{FFV}}(x) &= \frac{1}{6(x-1)^4} [-5x^4 + 14x^3 - 39x^2 + 38x - 8 + 18x^2 \ln x], \\
G_{\text{FFV}}(x) &= \frac{1}{(x-1)^3} [x^3 + 3x - 4 - 6x \ln x], \\
F_{\text{VVF}}(x) &= \frac{1}{6(x-1)^4} [4x^4 - 49x^3 + 78x^2 - 43x + 10 + 18x^3 \ln x], \\
G_{\text{VVF}}(x) &= \frac{1}{(x-1)^3} [-x^3 + 12x^2 - 15x + 4 - 6x^2 \ln x], \\
F_{\text{FFS}}(x) &= \frac{1}{6(x-1)^4} [x^3 - 6x^2 + 3x + 2 + 6x \ln x], \\
G_{\text{FFS}}(x) &= \frac{1}{(x-1)^3} [x^2 - 4x + 3 + 2 \ln x], \\
H_{\text{FFS}}(x) &= x[F_{\text{FFS}}(x) + G_{\text{FFS}}(x)], \\
F_{\text{SSF}}(x) &= \frac{1}{6(x-1)^4} [-2x^3 - 3x^2 + 6x - 1 + 6x^2 \ln x].
\end{aligned} \tag{52}$$

The results for one new field and two new fields with different spin in the loop are given in Tables 3 and 4, respectively. For new vector fermions, we retain only the leading contributions of $\mathcal{O}(\epsilon^2)$, where $\epsilon = Yv/M$ parametrizes the mixing between SM leptons and vector leptons.

Contributions to a_μ of two mixing vector fermions and SM bosons in the loop can be expressed as

$$\begin{aligned}
a_\mu^Z(F) &= \frac{G_F}{2\sqrt{2}\pi^2} \left[m_\mu^2 ((g_L^{ZF})^2 + (g_R^{ZF})^2) F_{\text{FFV}} \left(\frac{M_F^2}{M_Z^2} \right) + m_\mu M_F g_L^{ZF} g_R^{ZF} G_{\text{FFV}} \left(\frac{M_F^2}{M_Z^2} \right) \right], \\
a_\mu^W(N) &= \frac{G_F}{4\sqrt{2}\pi^2} \left[m_\mu^2 ((g_L^{WN})^2 + (g_R^{WN})^2) F_{\text{VVF}} \left(\frac{M_N^2}{M_W^2} \right) + m_\mu M_N g_L^{WN} g_R^{WN} G_{\text{VVF}} \left(\frac{M_N^2}{M_W^2} \right) \right], \\
a_\mu^H(F) &= \frac{G_F}{16\sqrt{2}\pi^2} \left[m_\mu^2 ((g_L^{HF})^2 + (g_R^{HF})^2) F_{\text{FFS}} \left(\frac{M_F^2}{M_H^2} \right) + m_\mu M_F g_L^{HF} g_R^{HF} G_{\text{FFS}} \left(\frac{M_F^2}{M_H^2} \right) \right],
\end{aligned} \tag{53}$$

where $F = \mu^-, \psi^-, \psi_D^-, \psi_A^-, \psi_T^-$ and $N = \psi^0, \psi_D^0, \psi_A^0, \psi_T^0$. The contributions of doubly-charged fermions are given by

$$\begin{aligned}
a_\mu^W(C) &= \frac{G_F}{4\sqrt{2}\pi^2} [m_\mu^2 ((g_L^{WC})^2 + (g_R^{WC})^2) \{ 2F_{\text{FFV}} \left(\frac{M_C^2}{M_W^2} \right) - F_{\text{VVF}} \left(\frac{M_C^2}{M_W^2} \right) \} \\
&\quad + m_\mu M_C g_L^{WC} g_R^{WC} \{ 2G_{\text{FFV}} \left(\frac{M_C^2}{M_W^2} \right) - G_{\text{VVF}} \left(\frac{M_C^2}{M_W^2} \right) \}],
\end{aligned} \tag{54}$$

Neutral vector boson (V^0)	$\frac{m_\mu^2(3g_L g_R - g_L^2 - g_R^2)}{12\pi^2 M_V^2}$
Charged vector boson (V^\pm)	$\frac{5m_\mu^2 g_R^2}{48\pi^2 M_V^2}$
Scalar doublet (ϕ_D)	$\frac{m_\mu^2 Y^2}{32\pi^2 M_\phi^2}$
Scalar triplet (ϕ_T)	$-\frac{3m_\mu^2 Y^2}{64\pi^2 M_\phi^2}$
Neutral vector fermion (ψ^0)	$\frac{G_F m_\mu^2 \epsilon^2}{24\sqrt{2}\pi^2} [-5 + 3F_{\text{VVF}}(M_\psi^2/M_W^2)]$
Charged vector fermion (ψ^\pm)	$\frac{G_F m_\mu^2 \epsilon^2}{16\sqrt{2}\pi^2} [-\frac{8}{3}c_W^2 + 2 + F_{\text{FFV}}(M_\psi^2/M_Z^2) + H_{\text{FFS}}(M_\psi^2/M_H^2)]$
Vector fermion doublet (ψ_D)	$\frac{G_F m_\mu^2 \epsilon^2}{16\sqrt{2}\pi^2} [\frac{8}{3}c_W^2 + \frac{4}{3} + F_{\text{FFV}}(M_\psi^2/M_Z^2) + H_{\text{FFS}}(M_\psi^2/M_H^2) + 2F_{\text{VVF}}(M_\psi^2/M_W^2) + 2G_{\text{VVF}}(M_\psi^2/M_W^2)]$
Vector fermion triplet (ψ_A)	$\frac{G_F m_\mu^2 \epsilon^2}{16\sqrt{2}\pi^2} [\frac{8}{3}c_W^2 - \frac{11}{3} + F_{\text{FFV}}(M_\psi^2/M_Z^2) + 2G_{\text{FFV}}(M_\psi^2/M_Z^2) + H_{\text{FFS}}(M_\psi^2/M_H^2) + F_{\text{VVF}}(M_\psi^2/M_W^2) + 2G_{\text{VVF}}(M_\psi^2/M_W^2)]$
Vector fermion triplet (ψ_T)	$\frac{G_F m_\mu^2 \epsilon^2}{32\sqrt{2}\pi^2} [-\frac{8}{3}c_W^2 - 18 + F_{\text{FFV}}(M_\psi^2/M_Z^2) + H_{\text{FFS}}(M_\psi^2/M_H^2) + 12F_{\text{VVF}}(M_\psi^2/M_W^2) + 4G_{\text{VVF}}(M_\psi^2/M_W^2) + 8F_{\text{FFV}}(M_\psi^2/M_W^2) + 8G_{\text{FFV}}(M_\psi^2/M_W^2)]$

Table 3: Correction δa_μ to the muon anomalous magnetic moment from one new field in the vertex loop. The functions F_{XYZ} , G_{XYZ} and H_{XYZ} are defined in (52). The notation follows the one introduced in Section 3.

with $C = \psi_T^{--}$. The couplings $g_{L,R}^{BF}$ of new vector fermions to muons and SM bosons (as induced by electroweak symmetry breaking) are defined as

$$\begin{aligned}
\mathcal{L} \supset & \frac{g}{\sqrt{2}} g_{L,R}^{WN} W_\mu^+ \bar{N} \gamma^\mu \mu_{L,R}^- + \frac{g}{\sqrt{2}} g_{L,R}^{WC} W_\mu^- \bar{C} \gamma^\mu \mu_{L,R}^- \\
& + \frac{g}{c_W} g_{L,R}^{ZF} Z_\mu \bar{F} \gamma^\mu \mu_{L,R}^- - \frac{1}{\sqrt{2}} g_{L,R}^{HF} \bar{F} \mu_{L,R}^- + \text{h.c.} .
\end{aligned} \tag{55}$$

For the different scenarios considered in this work, they are listed in Tables 5 and 6. We have expanded these couplings in terms of the mixing parameters $\epsilon_i = Y_i v/M_i$ and $\omega_{ij} = Y_{ij} v/(M_i - M_j)$, with $i = S, N, D, A, T$ and $ij = SD, DS$ etc. The respective Yukawa couplings are defined in (20)–(24) and (25)–(28). Our results agree with [17] for the case $\psi_D + \psi^\pm$. However, we find a different sign in front of the contribution with one doubly-charged fermion and two W bosons in the loop with respect to the one in (3.20) and (3.21) in [17].

$\phi^0 + \psi^\pm$	Fig. 4 (a)	$\frac{m_\mu^2 Y^2}{16\pi^2 M_\phi^2} F_{\text{FFS}}(M_\psi^2/M_\phi^2)$	$\delta a_\mu > 0$
$\phi^\pm + \psi^0$	Fig. 4 (b)	$\frac{m_\mu^2 Y^2}{16\pi^2 M_\phi^2} F_{\text{SSF}}(M_\psi^2/M_\phi^2)$	$\delta a_\mu < 0$
$\phi_D + \psi_D$	Fig. 4 (a,b)	$\frac{m_\mu^2 Y^2}{16\pi^2 M_\phi^2} [F_{\text{FFS}}(M_\psi^2/M_\phi^2) + F_{\text{SSF}}(M_\psi^2/M_\phi^2)]$	$\delta a_\mu > 0$
$\phi_D + \psi_A$	Fig. 4 (a,b)	$\frac{m_\mu^2 Y^2}{32\pi^2 M_\phi^2} [2F_{\text{FFS}}(M_\psi^2/M_\phi^2) + F_{\text{SSF}}(M_\psi^2/M_\phi^2)]$	$\delta a_\mu > 0$
$\phi_D + \psi_T$	Fig. 4 (a,e,f)	$\frac{m_\mu^2 Y^2}{32\pi^2 M_\phi^2} [5F_{\text{FFS}}(M_\psi^2/M_\phi^2) - 2F_{\text{SSF}}(M_\psi^2/M_\phi^2)]$	$\delta a_\mu > 0$
$\phi_A + \psi_D$	Fig. 4 (a,b)	$\frac{m_\mu^2 Y^2}{32\pi^2 M_\phi^2} [F_{\text{FFS}}(M_\psi^2/M_\phi^2) + 2F_{\text{SSF}}(M_\psi^2/M_\phi^2)]$	$\delta a_\mu < 0$
$\phi_A + \psi_T$	Fig. 4 (a,b,e,f)	$\frac{m_\mu^2 Y^2}{16\pi^2 M_\phi^2} 3F_{\text{FFS}}(M_\psi^2/M_\phi^2)$	$\delta a_\mu > 0$
$\phi_T + \psi_D$	Fig. 4 (b,c,d)	$\frac{m_\mu^2 Y^2}{32\pi^2 M_\phi^2} [-2F_{\text{FFS}}(M_\psi^2/M_\phi^2) + 5F_{\text{SSF}}(M_\psi^2/M_\phi^2)]$	$\delta a_\mu < 0$
$\phi_T + \psi_A$	Fig. 4 (a,b,c,d)	$\frac{m_\mu^2 Y^2}{16\pi^2 M_\phi^2} 3F_{\text{SSF}}(M_\psi^2/M_\phi^2)$	$\delta a_\mu < 0$
$V^0 + \psi^\pm$	Fig. 4 (g)	$\frac{m_\mu^2 g^2}{16\pi^2 M_V^2} F_{\text{FFV}}(M_\psi^2/M_V^2)$	$\delta a_\mu < 0$
$V^\pm + \psi^0$	Fig. 4 (h)	$\frac{m_\mu^2 g^2}{16\pi^2 M_V^2} F_{\text{VVF}}(M_\psi^2/M_V^2)$	$\delta a_\mu > 0$
$V_A + \psi_D$	Fig. 4 (g,h)	$\frac{m_\mu^2 g^2}{64\pi^2 M_V^2} [F_{\text{FFV}}(M_\psi^2/M_V^2) + 2F_{\text{VVF}}(M_\psi^2/M_V^2)]$	$\delta a_\mu > 0$

Table 4: Correction δa_μ from two new fields with different spin. The functions F_{XYZ} and G_{XYZ} are defined in (52). The notation follows the one introduced in Section 5.

B Four-lepton contact interactions

Four-lepton interactions are generated at the one-loop level by two new fields with different spin. The results for all combinations of fields defined in Table 1 that yield a positive contribution δa_μ are listed in Table 7. The corresponding loop functions read

$$\begin{aligned}
F_{\text{FS}}(x) &= \frac{1}{(x-1)^3} [x^2 - 1 - 2x \ln x], \\
F_{\text{FV}}(x) &= \frac{1}{(x-1)^3} [x^4 - 16x^3 + 19x^2 + 2(3x^2 + 4x - 4)x \ln x - 4].
\end{aligned}
\tag{56}$$

Notice that these results are model-independent and applicable to any scenario with couplings of two new fields to leptons.

References

- [1] J. Beringer *et al.* [Particle Data Group Collaboration], Phys. Rev. D **86**, 010001 (2012) and updates in fall 2013.
- [2] G. W. Bennett *et al.* [Muon G-2 Collaboration], Phys. Rev. D **73**, 072003 (2006) [hep-ex/0602035].

$\psi_D + \psi^\pm$	g_L^{BF}	g_R^{BF}
$Z\bar{\mu}^-\mu^-$	$-\frac{1}{2} + s_W^2 + \frac{\epsilon_S^2}{4}$	$s_W^2 - \frac{\epsilon_D^2}{4}$
$Z\bar{\psi}_D^-\mu^-$	$\frac{M_D\omega_{SD}-M_S\omega_{DS}}{4(M_S+M_D)}\epsilon_S$	$\frac{\epsilon_D}{2\sqrt{2}}$
$Z\bar{\psi}^-\mu^-$	$-\frac{\epsilon_S}{2\sqrt{2}}$	$\frac{M_S\omega_{SD}-M_D\omega_{DS}}{4(M_S+M_D)}\epsilon_D$
$W^+\bar{\nu}\mu^-$	$1 - \frac{\epsilon_S^2}{4}$	0
$W^+\bar{\psi}_D^0\mu^-$	$-\frac{m_\mu}{M_D}\frac{\epsilon_D}{\sqrt{2}} + \frac{(M_S-M_D)\omega_{SD}}{2M_D}\epsilon_S$	$-\frac{\epsilon_D}{\sqrt{2}}$
$H\bar{\mu}^-\mu^-$	$\sqrt{2}\frac{m_\mu}{M_H}$	$\sqrt{2}\frac{m_\mu}{M_H}$
$H\bar{\psi}_D^-\mu^-$	$\frac{m_\mu}{M_H}\epsilon_D + \frac{(M_D^2-2M_S^2)\omega_{SD}+M_SM_D\omega_{DS}}{\sqrt{2}M_H(M_S+M_D)}\epsilon_S$	$\frac{M_D}{M_H}\epsilon_D$
$H\bar{\psi}^-\mu^-$	$\frac{M_S}{M_H}\epsilon_S$	$\frac{m_\mu}{M_H}\epsilon_S + \frac{(2M_D^2-M_S^2)\omega_{SD}-M_SM_D\omega_{DS}}{\sqrt{2}M_H(M_S+M_D)}\epsilon_D$
$\psi_D + \psi^0$	g_L^{BF}	g_R^{BF}
$Z\bar{\mu}^-\mu^-$	$-\frac{1}{2} + s_W^2$	$s_W^2 - \frac{\epsilon_D^2}{4}$
$Z\bar{\psi}_D^-\mu^-$	0	$\frac{\epsilon_D}{2\sqrt{2}}$
$W^+\bar{\nu}\mu^-$	$1 - \frac{\epsilon_N^2}{4}$	0
$W^+\bar{\psi}_D^0\mu^-$	$-\frac{m_\mu}{M_D}\frac{\epsilon_D}{\sqrt{2}} + \frac{M_N(M_D\omega_{DN}-M_S\omega_{ND})}{2M_D(M_D+M_N)}\epsilon_N$	$-\frac{\epsilon_D}{\sqrt{2}}$
$W^+\bar{\psi}^0\mu^-$	$\frac{\epsilon_N}{\sqrt{2}}$	$\frac{M_D\omega_{DN}-M_S\omega_{ND}}{2(M_D+M_N)}\epsilon_D$
$H\bar{\mu}^-\mu^-$	$\sqrt{2}\frac{m_\mu}{M_H}$	$\sqrt{2}\frac{m_\mu}{M_H}$
$H\bar{\psi}_D^-\mu^-$	$\frac{m_\mu}{M_H}\epsilon_D$	$\frac{M_D}{M_H}\epsilon_D$

Table 5: Couplings $g_{L,R}^{BF}$ of a new fermion F and a SM boson B to a left- or right-handed muon in scenarios with mixing vector fermion doublet and singlet in the vertex loop.

- [3] F. Jegerlehner and A. Nyffeler, Phys. Rept. **477**, 1 (2009) [arXiv:0902.3360 [hep-ph]].
- [4] G. Venanzoni [Fermilab E989 Collaboration], Frascati Phys. Ser. **56**, 195 (2012).
- [5] N. Saito [J-PARC g-2/EDM Collaboration], AIP Conf. Proc. **1467**, 45 (2012).
- [6] M. Davier, A. Hoecker, B. Malaescu and Z. Zhang, Eur. Phys. J. C **71**, 1515 (2011) [Erratum-ibid. C **72**, 1874 (2012)] [arXiv:1010.4180 [hep-ph]];
K. Hagiwara, R. Liao, A. D. Martin, D. Nomura and T. Teubner, J. Phys. G **38**, 085003 (2011) [arXiv:1105.3149 [hep-ph]];
M. Benayoun, P. David, L. DelBuono and F. Jegerlehner, Eur. Phys. J. C **73**, 2453 (2013) [arXiv:1210.7184 [hep-ph]].
- [7] P. Fayet, Phys. Rev. D **75**, 115017 (2007) [hep-ph/0702176];
M. Pospelov, Phys. Rev. D **80**, 095002 (2009) [arXiv:0811.1030 [hep-ph]].

$\psi_D + \psi_A$	g_L^{BF}	g_R^{BF}
$Z\bar{\mu}^-\mu^-$	$-\frac{1}{2} + s_W^2 - \frac{\epsilon_A^2}{4}$	$s_W^2 - \frac{\epsilon_D^2}{4}$
$Z\bar{\psi}_D^-\mu^-$	$\frac{M_A\omega_{DA}-M_D\omega_{AD}}{4(M_D+M_A)}\epsilon_A$	$\frac{\epsilon_D}{2\sqrt{2}}$
$Z\bar{\psi}_A^-\mu^-$	$\frac{\epsilon_A}{2\sqrt{2}}$	$\frac{m_\mu}{M_A}\frac{\epsilon_A}{\sqrt{2}} + \frac{(2M_D^2-M_A^2)\omega_{AD}-M_AM_D\omega_{DA}}{4M_A(M_D+M_A)}\epsilon_D$
$W^+\bar{\nu}\mu^-$	$1 + \frac{\epsilon_A^2}{8}$	0
$W^+\bar{\psi}_D^0\mu^-$	$-\frac{m_\mu}{M_D}\frac{\epsilon_D}{\sqrt{2}} + \frac{M_A(M_A\omega_{AD}-M_D\omega_{DA})}{4M_D(M_D+M_A)}\epsilon_A$	$-\frac{\epsilon_D}{\sqrt{2}}$
$W^+\bar{\psi}_A^0\mu^-$	$-\frac{\epsilon_A}{2}$	$-\frac{m_\mu}{M_A}\epsilon_A - \frac{(2M_D^2-M_A^2)\omega_{AD}-M_AM_D\omega_{DA}}{2\sqrt{2}M_A(M_D+M_A)}\epsilon_D$
$H\bar{\mu}^-\mu^-$	$\sqrt{2}\frac{m_\mu}{M_H}$	$\sqrt{2}\frac{m_\mu}{M_H}$
$H\bar{\psi}_D^-\mu^-$	$\frac{m_\mu}{M_H}\epsilon_D + \frac{(M_D^2-2M_A^2)\omega_{AD}+M_AM_D\omega_{DA}}{\sqrt{2}M_H(M_D+M_A)}\epsilon_A$	$\frac{M_D}{M_H}\epsilon_D$
$H\bar{\psi}_A^-\mu^-$	$\frac{M_A}{M_H}\epsilon_A$	$\frac{m_\mu}{M_H}\epsilon_A + \frac{(2M_D^2-M_A^2)\omega_{AD}-M_AM_D\omega_{DA}}{\sqrt{2}M_H(M_D+M_A)}\epsilon_D$
$\psi_D + \psi_T$	g_L^{BF}	g_R^{BF}
$Z\bar{\mu}^-\mu^-$	$-\frac{1}{2} + s_W^2 + \frac{\epsilon_T^2}{8}$	$s_W^2 - \frac{\epsilon_D^2}{4}$
$Z\bar{\psi}_D^-\mu^-$	$\frac{M_D\omega_{TD}-M_T\omega_{DT}}{8(M_D+M_T)}\epsilon_T$	$\frac{\epsilon_D}{2\sqrt{2}}$
$Z\bar{\psi}_T^-\mu^-$	$\frac{\epsilon_T}{4}$	$\frac{M_D\omega_{DT}-M_T\omega_{TD}}{4\sqrt{2}(M_D+M_T)}\epsilon_D$
$W^+\bar{\nu}\mu^-$	$1 - \frac{7\epsilon_T^2}{8}$	0
$W^+\bar{\psi}_D^0\mu^-$	$-\frac{m_\mu}{M_D}\frac{\epsilon_D}{\sqrt{2}} - \frac{(3M_D^2+M_T^2)\omega_{TD}-4M_TM_D\omega_{DT}}{4M_D(M_D+M_T)}\epsilon_T$	$-\frac{\epsilon_D}{\sqrt{2}}$
$W^+\bar{\psi}_T^0\mu^-$	$\sqrt{2}\epsilon_T$	$\frac{m_\mu}{M_T}\frac{\epsilon_T}{\sqrt{2}} - \frac{(2M_T^2-M_D^2)\omega_{TD}-M_TM_D\omega_{DT}}{2M_T(M_D+M_T)}\epsilon_D$
$W^+\bar{\psi}_T^-\mu^-$	$-\frac{\epsilon_T}{\sqrt{2}}$	$-\frac{m_\mu}{M_T}\frac{\epsilon_T}{\sqrt{2}} - \frac{(M_D-M_T)\omega_{TD}}{2M_T}\epsilon_D$
$H\bar{\mu}^-\mu^-$	$\sqrt{2}\frac{m_\mu}{M_H}$	$\sqrt{2}\frac{m_\mu}{M_H}$
$H\bar{\psi}_D^-\mu^-$	$\frac{m_\mu}{M_H}\epsilon_D + \frac{(M_D^2-2M_T^2)\omega_{TD}+M_TM_D\omega_{DT}}{2\sqrt{2}M_H(M_D+M_T)}\epsilon_T$	$\frac{M_D}{M_H}\epsilon_D$
$H\bar{\psi}_T^-\mu^-$	$-\frac{M_T}{M_H}\frac{\epsilon_T}{\sqrt{2}}$	$-\frac{m_\mu}{M_H}\frac{\epsilon_T}{\sqrt{2}} - \frac{(2M_D^2-M_T^2)\omega_{TD}-M_TM_D\omega_{DT}}{2M_H(M_D+M_T)}\epsilon_D$

Table 6: Couplings $g_{L,R}^{BF}$ of a new fermion F and a SM boson B to a left- or right-handed muon in scenarios with mixing vector fermion doublet and triplet in the vertex loop.

$\phi^0 + \psi^\pm$	–	0
$\phi_D + \psi_D$	Fig. 5 (a)	$\frac{Y^4}{64\pi^2 M_\phi^2} F_{\text{FS}}(M_\psi^2/M_\phi^2) \mathcal{O}_{\text{RR}}$
$\phi_D + \psi_A$	Fig. 5 (a)	$\frac{(Y/\sqrt{2})^4}{64\pi^2 M_\phi^2} F_{\text{FS}}(M_\psi^2/M_\phi^2) \mathcal{O}_{\text{LL}}$
$\phi_D + \psi_T$	Fig. 5 (b)	$\frac{Y^4}{64\pi^2 M_\phi^2} F_{\text{FS}}(M_\psi^2/M_\phi^2) \mathcal{O}_{\text{LL}}$
$\phi_A + \psi_T$	–	0
$V^\pm + \psi^0$	Fig. 5 (c)	$\frac{g^4}{64\pi^2 M_V^2} F_{\text{FV}}(M_\psi^2/M_V^2) \mathcal{O}_{\text{RR}}$
$V_A + \psi_D$	Fig. 5 (c,d)	$\frac{g^4}{256\pi^2 M_V^2} [F_{\text{FV}}(M_\psi^2/M_V^2) - 3F_{\text{FS}}(M_\psi^2/M_V^2)] \mathcal{O}_{\text{LL}}$

Table 7: Effective four-lepton interactions $\mathcal{C}_{AA}\mathcal{O}_{AA}$ for pairs of new fields leading to $\delta a_\mu > 0$. The loop functions F_{FS} and F_{FV} are defined in (56). The notation has been introduced in Section 5.

- H. Davoudiasl, H.-S. Lee and W. J. Marciano, Phys. Rev. D **86**, 095009 (2012) [arXiv:1208.2973 [hep-ph]].
- [8] M. E. Peskin and T. Takeuchi, Phys. Rev. D **46**, 381 (1992).
- [9] J. Baron *et al.* [ACME Collaboration], Science **343**, 269 (2014) [arXiv:1310.7534 [physics.atom-ph]].
- [10] V. Cirigliano, B. Grinstein, G. Isidori and M. B. Wise, Nucl. Phys. B **728**, 121 (2005) [hep-ph/0507001].
- [11] T. Hahn, Comput. Phys. Commun. **140**, 418 (2001) [hep-ph/0012260].
- [12] A. Czarnecki and B. Krause, Nucl. Phys. Proc. Suppl. **51C**, 148 (1996) [hep-ph/9606393].
- [13] R. Mertig, M. Böhm and A. Denner, Comput. Phys. Commun. **64**, 345 (1991).
- [14] A. Belyaev, N. D. Christensen and A. Pukhov, Comput. Phys. Commun. **184**, 1729 (2013) [arXiv:1207.6082 [hep-ph]].
- [15] J. Alcaraz *et al.* [ALEPH and DELPHI and L3 and OPAL and LEP Electroweak Working Group Collaborations], hep-ex/0612034.
- [16] G. Abbiendi *et al.* [OPAL Collaboration], Eur. Phys. J. C **13**, 553 (2000) [hep-ex/9908008].
- [17] K. Kannike, M. Raidal, D. M. Straub and A. Strumia, JHEP **1202**, 106 (2012) [Erratum-ibid. **1210**, 136 (2012)] [arXiv:1111.2551 [hep-ph]].
- [18] R. Dermisek and A. Raval, Phys. Rev. D **88**, 013017 (2013) [arXiv:1305.3522 [hep-ph]].

- [19] F. del Aguila, J. de Blas and M. Perez-Victoria, Phys. Rev. D **78**, 013010 (2008) [arXiv:0803.4008 [hep-ph]].
- [20] M. E. Peskin and T. Takeuchi, Phys. Rev. D **46**, 381 (1992).
- [21] T. Aoyama, M. Hayakawa, T. Kinoshita and M. Nio, Phys. Rev. Lett. **109**, 111807 (2012) [arXiv:1205.5368 [hep-ph]].
- [22] ATLAS collaboration, ATLAS-CONF-2013-035.
- [23] CMS collaboration, CMS-PAS-SUS-13-006.
- [24] ATLAS collaboration, ATLAS-CONF-2013-019.
- [25] S. Chatrchyan *et al.* [CMS Collaboration], Phys. Lett. B **718**, 348 (2012) [arXiv:1210.1797 [hep-ex]].
- [26] ATLAS collaboration, ATLAS-CONF-2013-049.
- [27] CMS collaboration, arXiv:1307.7135 [hep-ex].
- [28] J. L. Lopez, D. V. Nanopoulos and X. Wang, Phys. Rev. D **49**, 366 (1994) [hep-ph/9308336];
U. Chattopadhyay and P. Nath, Phys. Rev. D **53**, 1648 (1996) [hep-ph/9507386].
- [29] T. Moroi, Phys. Rev. D **53**, 6565 (1996) [Erratum-ibid. D **56**, 4424 (1997)] [hep-ph/9512396].
- [30] M. Endo, K. Hamaguchi, S. Iwamoto and T. Yoshinaga, JHEP **1401**, 123 (2014) [arXiv:1303.4256 [hep-ph]];
S. Mohanty, S. Rao and D. P. Roy, JHEP **1309**, 027 (2013) [arXiv:1303.5830 [hep-ph]];
M. Ibe, T. T. Yanagida and N. Yokozaki, JHEP **1308**, 067 (2013) [arXiv:1303.6995 [hep-ph]];
A. Fowlie, K. Kowalska, L. Roszkowski, E. M. Sessolo and Y.-L. S. Tsai, Phys. Rev. D **88**, 055012 (2013) [arXiv:1306.1567 [hep-ph]].
- [31] T. Han, I. -W. Kim and J. Song, Phys. Lett. B **693**, 575 (2010) [arXiv:0906.5009 [hep-ph]]; N. Christensen, T. Han, J. Song and Stefanus, in preparation.